

# Optical Pulse Storage Rings and Transmission Systems

by

William Siu-Cheong Wong

Submitted to the Department of  
Electrical Engineering and Computer Science  
in partial fulfillment of the requirements for the degree of

Master of Science  
in Electrical Engineering and Computer Science

at the

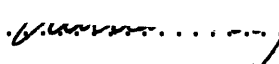
MASSACHUSETTS INSTITUTE OF TECHNOLOGY

May 1995


© Massachusetts Institute of Technology 1995. All rights reserved. MASSACHUSETTS INSTITUTE OF TECHNOLOGY

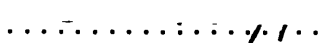
JUL 17 1995

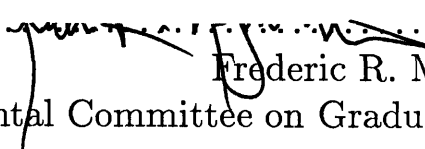
LIBRARIES

Author .....  .....  
Department of  
Electrical Engineering and Computer Science  
May 12, 1995

Barker Eng

Certified by .....  .....  
Hermann A. Haus  
Institute Professor  
Thesis Supervisor

Certified by .....  .....  
Erich P. Ippen  
Elihu Thomson Professor of Electrical Engineering  
Thesis Supervisor

Accepted by .....  .....  
Frederic R. Morgenthaler  
Chairman, Departmental Committee on Graduate Students

# Optical Pulse Storage Rings and Transmission Systems

by

William Siu-Cheong Wong

Submitted to the Department of  
Electrical Engineering and Computer Science  
on May 12, 1995, in partial fulfillment of the  
requirements for the degree of  
Master of Science  
in Electrical Engineering and Computer Science

## Abstract

We study the effectiveness of compensation techniques, including intensity-dependent gain/absorption, filtering, and amplitude- and phase-modulation, in combating amplifier noise in high bit rate (10+ Gb/s) pulse storage rings and transmission systems. At these high rates, we find that in the absence of compensation, the noise-imparted limitation due to the self-Raman frequency shift can exceed the Gordon-Haus effect. Optical storage ring operation is demonstrated experimentally at 1 GHz where a data packet is maintained for as long as 30 minutes.

Thesis Supervisor: Hermann A. Haus  
Title: Institute Professor

Thesis Supervisor: Erich P. Ippen  
Title: Elihu Thomson Professor of Electrical Engineering

## Acknowledgements

I thank my thesis supervisors Professors Hermann A. Haus and Erich P. Ippen for the opportunity to work in their research group. I am grateful to both of them for financial support through a research assistantship.

I thank Professor Haus for listening to my ideas patiently during the past two years. His unsurpassed creativity and productivity has been inspiring. Professor Ippen always guided me through research problems by offering his intuitive pictures. His insight, comments, as well as his penetrating questions are greatly appreciated.

It has been a true pleasure working with Dr. John Moores, who also wrote two sections of Chapter 3. I also enjoyed working with Farzana Khatri on the soliton-continuum problem. I thank both of them for being my close friends and for finding time to listen to my personal problems.

I thank Dr. Christopher Doerr for his help when I first started working with optical fibers in the lab. I thank my former office mates Jerry Chen and Lynn Nelson for their friendship and for explaining to me how the bureaucratic machine of MIT works. Sharing an office with Constantine Tziligakis and Andrew Ugarov has been enjoyable.

Thanks to Group 67 of the MIT Lincoln Laboratory for the opportunity to work on high bit-rate TDM systems. I am grateful to Dr. Katie Hall for teaching me useful laboratory skills and lending me equipment; to Dr. John Moores for escorting me inside Lincoln Laboratory and sharing his ideas with me; to Suzanne LePage and Claudia Fennelly for providing much needed experimental help; and to Dr. Kristin Rauschenbach, Eric Swanson, Dr. Roy Bondurant, and Dr. Vincent Chan for their advice and leadership.

I thank John Oliver and William Cutter of the MIT Concert Choir for their guidance and patience with the chorus. Their dedication and efforts have certainly made my experience at MIT an enjoyable one.

Kohichi Tamura has been a loyal friend to me. Thanks to my roommate Jason Ho for putting up with my random sleeping hours, and to Sophia for her friendship

and great tacos.

My parents and my brother Thompson have been my sources of strength and confidence. I thank Nini for all her love and understanding, and I look forward to spending the rest of my life with her.

# Contents

<b>1</b>	<b>Introduction</b>	<b>10</b>
1.1	Soliton Transmission and Storage . . . . .	10
1.2	The All-Optical Network Consortium . . . . .	11
1.3	Organization of Thesis . . . . .	12
<b>2</b>	<b>Wave Propagation in Optical Fibers</b>	<b>13</b>
2.1	Linear Dispersion . . . . .	14
2.2	Self-Phase Modulation . . . . .	16
2.3	Optical Solitons . . . . .	17
2.4	Nonlinear Polarization Rotation . . . . .	18
<b>3</b>	<b>Stability and Timing Maintenance in Soliton Transmission and Storage Rings</b>	<b>21</b>
3.1	Model . . . . .	22
3.2	Stability of Zeros . . . . .	28
3.2.1	Systems with Amplitude Modulation and Filtering . . . . .	30
3.2.2	Systems with Phase Modulation and Filtering . . . . .	30
3.3	The ONEs . . . . .	31
3.3.1	Soliton Perturbation Theory . . . . .	31
3.3.2	Evolution of Uncompensated Systems . . . . .	37
3.3.2.1	Classical . . . . .	37
3.3.2.2	Stochastic . . . . .	38

3.3.3	Evolution of Systems Compensated with Phase Modulation and Filtering . . . . .	40
3.3.3.1	Classical . . . . .	41
3.3.3.2	Stochastic . . . . .	43
3.3.3.3	Numerical Simulation . . . . .	44
3.3.4	Evolution of Systems Compensated with Intensity-dependent Absorption/Gain, Amplitude Modulation, and Filtering . . . . .	46
3.3.4.1	Case I: Filtering, AM, and FSA/G . . . . .	46
3.3.4.2	Case II: FSA+G, AM, and Filtering . . . . .	48
<b>4</b>	<b>Experimental Demonstration of an Optical Memory</b>	<b>52</b>
4.1	Additive-pulse Modelocking/Limiting . . . . .	52
4.2	Experimental Setup . . . . .	54
<b>5</b>	<b>Conclusions and Future Work</b>	<b>58</b>
<b>A</b>	<b>Normalizing the Evolution Equation</b>	<b>60</b>
A.1	Master Equation with Group Velocity Dispersion . . . . .	60
A.2	Master Equation near Zero Group Velocity Dispersion Point . . . . .	64

# List of Figures

1-1	Pulse storage ring design as suggested by Haus and Mecozzi. . . . .	11
1-2	The all-optical network architecture, courtesy of MIT Lincoln Laboratory. . . . .	12
2-1	Dispersion of single-mode fiber vs. wavelength for different material composition and modefield diameter, after Ref. [1]. Note that the dispersion parameter is defined as $D = -\frac{2\pi c}{\lambda^2}\beta''(\omega_0)$ . . . . .	16
2-2	The additive-pulse modelocking action through nonlinear polarization rotation. . . . .	19
2-3	Plot of intracavity transmission vs. normalized intensity. . . . .	20
3-1	$\omega_0$ is the initial carrier frequency of the solitons, $(\omega_0 - p)$ is the actual carrier frequency of a soliton, and $\omega_{f0}$ is the difference between $\omega_0$ and the filter center frequency. . . . .	25
3-2	Cubic fit to effective gain vs. intensity with interferometric FSG+A+G. . . . .	26
3-3	Theoretical stability diagram for soliton storage ring with amplitude modulation and filtering. . . . .	31
3-4	Theoretical stability diagram for soliton storage ring with phase modulation and filtering. Note that the system is marginally stable with no filtering (along the horizontal axis). . . . .	32

3-5	Normalized timing variance. Variance of 25 single-pulse simulations - solid curve. Dotted curve - perturbation theory. Pulse FWHM = 0.1 ps, $D' = 0.5$ ps/nm/km. Note that the curve changes its slope from +3 to +5 at approximately $z = 20z_0$ , which in this example is approximately 16 km. . . . .	41
3-6	Pulse transmission through a phase modulator, after Ref. [2]. Note that $2\Delta_m = M_{PM}$ . . . . .	42
3-7	An analogous system where the position of the point mass evolves according to Eq. (3.57). . . . .	43
3-8	111 Gb/s soliton data in storage ring with and without compensation (phase modulation and filtering). Parameters in text. . . . .	45
3-9	Transmission vs. intensity curves for the intensity-dependent absorption of Case I. Solid=FSA case. Dashed=FSG case. Circle indicates peak initial intensity. Square indicates peak intensity at 50 km. . . .	47
3-10	Schematic of Case I storage loop. . . . .	48
3-11	Case I with FSG. The initial ONEs broadened and became less intense. The ZEROs were observed to grow; two of them eventually becoming false ONEs. . . . .	49
3-12	Case I with FSA. The ZEROs were stable while the intensities of the ONEs fluctuated greatly, to the extent that one of the pulses was extinguished. . . . .	50
3-13	Transmission vs. intensity of the intensity-dependent absorption of Case II. Square indicates steady-state peak intensity. . . . .	50
3-14	Simulation to 25 km. Solid: Case II with FSA+G. Dashed: Case I with FSG. . . . .	51
4-1	The additive-pulse limiting (APL) laser, after Ref. [3]. . . . .	53
4-2	A random pulse pattern is maintained in the APL laser. The modulator frequency is 510 MHz (17 times the round-trip frequency). The horizontal scale is 5 ns/division, after Ref. [3]. . . . .	53



4-3	Experimental setup: EDFA, erbium-doped fiber amplifier; SA, semiconductor amplifier; PBS, polarization beam splitter; $\lambda/2$ , $\lambda/4$ , half-wave and quarter-wave plates. . . . .	54
4-4	Example of loading data into a storage ring by use of a 90 ns electrical gating pulse. Horizontal scale, 500 ps/division. . . . .	56
4-5	Optical Spectra of the PPG and the PSR. . . . .	57
5-1	The figure-eight laser. . . . .	59

# Chapter 1

## Introduction

### 1.1 Soliton Transmission and Storage

In 1973, Hasegawa and Tappert [4] first proposed the idea of using optical solitons in fiber communication systems. They suggested using the nonlinearity of the fiber medium to compensate for the group-velocity dispersion of pulses. However, because of material loss, the pulse width increases in the course of propagation. One solution is to use periodic amplification to maintain the pulse shape via the stimulated Raman process [5–7].

Another solution came in 1990 when Desurvire and his coworkers perfected the erbium-doped fiber amplifier [8]. When the  $\text{Er}^{3+}$  ions in the glass host are excited to a higher energy state by a pump source, they can amplify incident light at  $1.5 \mu\text{m}$  with a bandwidth of about 50 nm.

Using the above two technologies, Nakazawa achieved error-free soliton data transmission over unlimited distances [9, 10]. Inspired by the Nakazawa's experiments, Haus and Mecozzi suggested the idea of storing a bit stream of solitons (ONEs) and gaps (ZEROs) in a ring configuration [11]. Their design was shown in Figure 1-1, where the bit stream recirculated in a fiber ring. The system consisted of an optical amplifier to compensate loss, an amplitude modulator to maintain pulse timing, and a bandpass filter to minimize frequency jitter. They were able to show, using soliton perturbation theory [12, 13], that there existed a regime of operation such that both

the ONEs (pulses) and the ZEROs (the absence of a pulse) are stable.

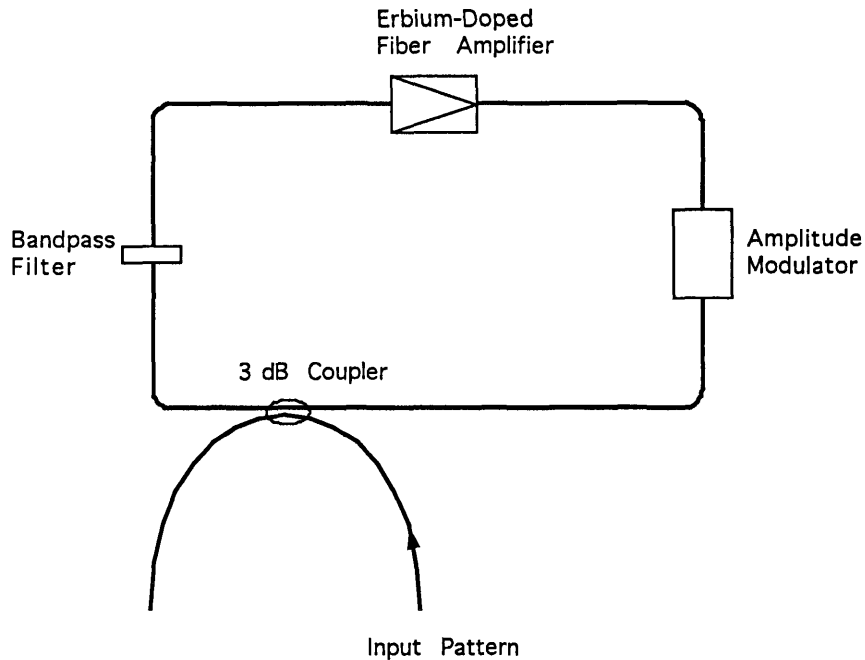


Figure 1-1: Pulse storage ring design as suggested by Haus and Mecozzi.

## 1.2 The All-Optical Network Consortium

In 1993, AT&T, DEC, and MIT formed a pre-competitive consortium on wide-band all-optical networks to develop a national information infrastructure using fiber-optic technology [14]. The network architecture, which is all-optical, is shown in Figure 1-2.

The 100 Gb/s local area network (LAN) uses time-division multiplexing (TDM) technology [15], where packets are routed from node to node until they arrive at the proper receiving node. This slotted TDM technology allows various optical terminals to operate at different speeds. For example, video images, computer data, and voice can be transmitted and received at the same time. An all-optical gateway links this TDM LAN to a wide area network (WAN). To minimize pulse degradation over the long propagation distances in the WAN, the gateway converts the high bit-rate stream from the LAN to multiple lower bit-rate streams where the pulses are broader. This is known as wavelength-division multiplexing (WDM), since each stream in the WAN is centered at a different wavelength.

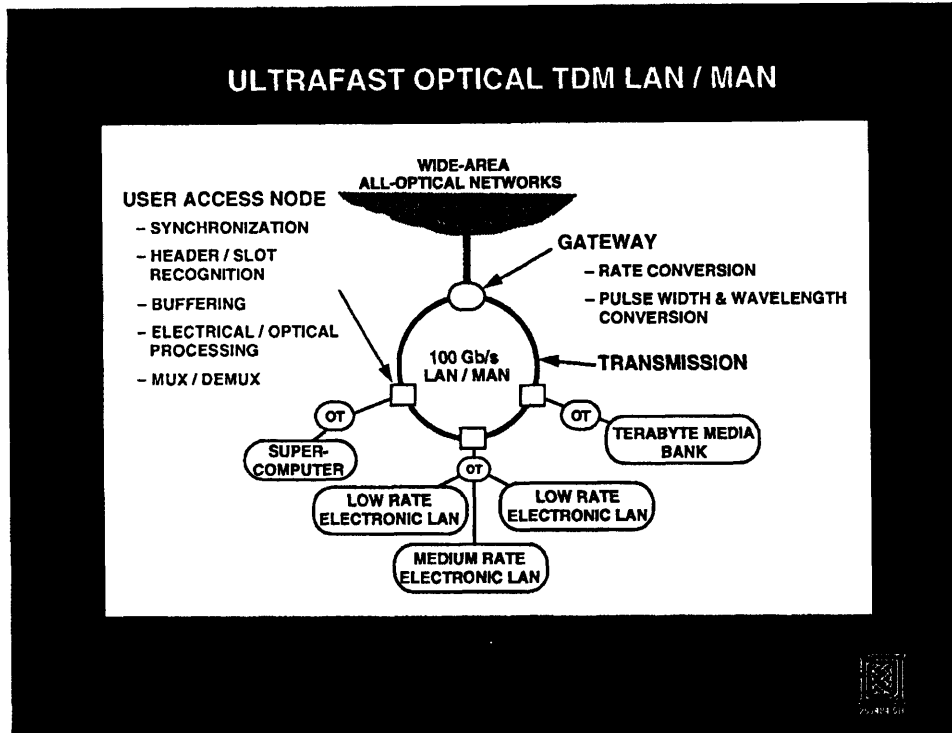


Figure 1-2: The all-optical network architecture, courtesy of MIT Lincoln Laboratory.

Optical buffers are needed to perform rate conversion at the all-optical gateway. For example, in order to demultiplex a high bit-rate incoming packet into  $N$  lower bit-rate streams, the packet is required to circulate in the optical buffer for a minimum of  $N$  roundtrips. In addition, buffers can be used to mediate collisions between multiple packets arriving at a particular node simultaneously.

### 1.3 Organization of Thesis

This thesis is organized as follows. Phenomena encountered in pulse propagation in an optical fiber, such as dispersion, self-phase modulation, and nonlinear polarization rotation, are introduced in Chapter 2. Timing maintenance of the ONEs and the stability of the ZEROs in an optical storage ring are studied in Chapter 3. An experimental demonstration of optical storage ring operation — loading, storing, and unloading packet data is discussed in Chapter 4. The thesis ends with conclusions and future work in Chapter 5.

## Chapter 2

# Wave Propagation in Optical Fibers

In this chapter, we present the theory of light propagation in an optical fiber. We will develop a mathematical model to describe the evolution of the envelope of a wavepacket in a dispersive medium where the refractive index depends on the field intensity.

We first begin with Maxwell's equations with no sources in an isotropic medium [16],

$$\nabla \cdot \mathbf{D}(\mathbf{r}, t) = 0 \quad (2.1)$$

$$\nabla \cdot \mathbf{B}(\mathbf{r}, t) = 0 \quad (2.2)$$

$$\nabla \times \mathbf{E}(\mathbf{r}, t) = -\frac{\partial \mathbf{B}(\mathbf{r}, t)}{\partial t} \quad (2.3)$$

$$\nabla \times \mathbf{H}(\mathbf{r}, t) = \frac{\partial \mathbf{D}(\mathbf{r}, t)}{\partial t} \quad (2.4)$$

We can obtain a single partial differential equation for the propagation of the electric field by taking the curl of Eq. (2.3), and using Eqs. (2.1) and (2.4)

$$\nabla^2 \mathbf{E}(\mathbf{r}, t) - \frac{1}{c^2} \frac{\partial^2 \mathbf{E}(\mathbf{r}, t)}{\partial t^2} = \frac{1}{\epsilon_0 c^2} \frac{\partial^2 \mathbf{P}(\mathbf{r}, t)}{\partial t^2} . \quad (2.5)$$

## 2.1 Linear Dispersion

Since the polarization field in an optical fiber does not respond instantaneously to incident light, that is,

$$\mathbf{P}(z, t) = \epsilon_0 \int_{-\infty}^{+\infty} \chi(t - \tau) \mathbf{E}(z, \tau) d\tau , \quad (2.6)$$

the susceptibility  $\chi(\omega)$  is frequency-dependent. Because of causality, the real and imaginary parts of  $\chi(\omega)$  are Hilbert transform pairs

$$\chi_1(\omega) = \frac{1}{\pi} \text{P} \int_{-\infty}^{+\infty} \frac{\chi_2(\omega') d\omega'}{\omega' - \omega} , \quad (2.7)$$

$$\chi_2(\omega) = -\frac{1}{\pi} \text{P} \int_{-\infty}^{+\infty} \frac{\chi_1(\omega') d\omega'}{\omega' - \omega} . \quad (2.8)$$

The real part  $\chi_1(\omega)$  modifies the propagation speed, whereas the imaginary part  $\chi_2(\omega)$  determines the absorption or amplification by the medium. Using the linear dispersion relation

$$\mathbf{D}(z, \omega) = \epsilon_0 \mathbf{E}(z, \omega) + \mathbf{P}(z, \omega) = \epsilon_0(\omega) [1 + \chi(\omega)] \mathbf{E}(z, \omega) , \quad (2.9)$$

we can rewrite the wave equation (2.5) in the Fourier domain for an axially uniform optical fiber as

$$\nabla^2 \mathbf{E}(\mathbf{r}, \omega) + \omega^2 \mu \epsilon(\rho, \omega) \mathbf{E}(\mathbf{r}, \omega) = 0 , \quad (2.10)$$

where  $\mu \epsilon(\rho, \omega) = [1 + \chi(\rho, \omega)] / c^2$  and  $\rho = \sqrt{x^2 + y^2}$ .

If the electric field is  $y$ -polarized and it propagates along the  $z$ -direction, we can write

$$\mathbf{E}(\mathbf{r}, t) = \hat{\mathbf{y}} a(x, y) e^{j(\omega t - \beta(\omega)z)} . \quad (2.11)$$

Substituting Eq. (2.11) into the wave equation (2.10), we obtain a differential equation that defines the transverse eigenmode  $a(x, y)$  in the optical fiber with modal

propagation constant  $\beta(\omega)$ ,

$$\nabla_{\mathbf{T}}^2 a(x, y) + [\omega^2 \mu \epsilon(\rho, \omega) - \beta^2(\omega)] a(x, y) = 0. \quad (2.12)$$

The evolution in  $z$  can be obtained by assuming

$$\mathbf{E}(\mathbf{r}, \omega) = \hat{\mathbf{y}} E(z, \omega) a(x, y) \quad (2.13)$$

in Eq. (2.10), which yields a scalar partial differential equation,

$$\frac{\partial^2 E(z, \omega)}{\partial z^2} + \beta^2(\omega) E(z, \omega) = 0. \quad (2.14)$$

The modal propagation constant  $\beta(\omega)$  depends on frequency in a complicated way, because apart from resonance contributions, waveguide dispersion also plays a significant role. To simplify calculations, we perform a Taylor series expansion of  $\beta(\omega)$  around the optical carrier frequency  $\omega_0$  away from electronic resonances,

$$\beta(\omega) = \beta(\omega_0) + \beta'(\omega_0) (\omega - \omega_0) + \frac{1}{2} \beta''(\omega_0) (\omega - \omega_0)^2 + \dots. \quad (2.15)$$

The envelope of the wavepacket moves at the group velocity  $v_{\text{group}} = 1/\beta'(\omega_0)$ . The parameter  $\beta''(\omega_0)$  describes pulse broadening due to dispersion. We can “factorize” and rewrite Eq. (2.14) in the time domain (dropping the term containing  $\beta(\omega_0)$ ) as

$$\frac{\partial E(z, t)}{\partial z} + \frac{1}{v_{\text{group}}} \frac{\partial E(z, t)}{\partial t} = \frac{j}{2} \beta''(\omega_0) \frac{\partial^2 E(z, t)}{\partial t^2}. \quad (2.16)$$

Instead of solving Eq. (2.5), a vector partial differential equation in  $3 + 1$  dimensions, we have greatly simplified the problem such that we can now work with Eq. (2.16), a scalar partial differential equation in  $1 + 1$  dimensions.

In Figure 2-1, the dispersion of single-mode fiber is shown for different material composition and modefield diameter.

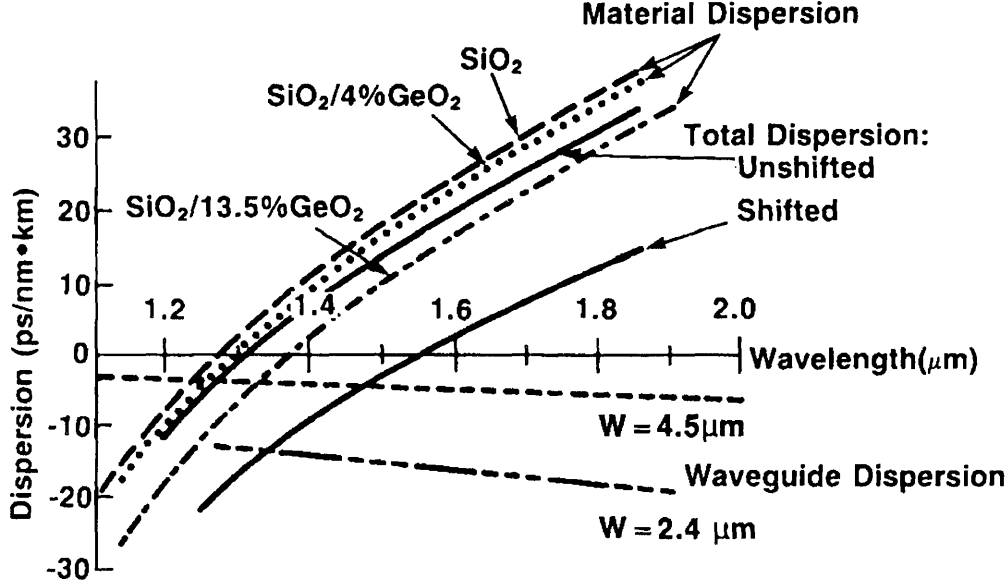


Figure 2-1: Dispersion of single-mode fiber vs. wavelength for different material composition and modefield diameter, after Ref. [1]. Note that the dispersion parameter is defined as  $D = -\frac{2\pi c}{\lambda^2}\beta''(\omega_0)$ .

## 2.2 Self-Phase Modulation

The response of an isotropic optical fiber to an external electric field becomes nonlinear when the field is intense (comparable to the internal atomic field). This nonlinearity originates from the anharmonic motion of bound electrons under the influence of an applied field. Self-phase modulation, one of the nonlinear effects, can be modeled as

$$\mathbf{P}^{\text{NL}}(z, \omega) = \epsilon_0 \chi^{(3)} |\mathbf{E}(z, \omega)|^2 \mathbf{E}(z, \omega) \quad (2.17)$$

where  $\chi^{(3)}$  is real and positive.

What happens physically is that the refractive index becomes dependent on the optical intensity. As a result, when an optical pulse propagates, its peak will acquire more phase shift than its wings will. Self-phase modulation plays an essential role in optical soliton formation. One can incorporate this nonlinearity into the wave equation by defining

$$\mathbf{D}(z, \omega) = \epsilon_0(\omega) [1 + \chi^{(1)}(\omega)] \mathbf{E}(z, \omega) + \mathbf{P}^{\text{NL}}(z, \omega), \quad (2.18)$$



which yields the cubic nonlinear Schrödinger equation

$$\frac{\partial E(z, t)}{\partial z} + \frac{1}{v_{\text{group}}} \frac{\partial E(z, t)}{\partial t} - \frac{j}{2} \beta''(\omega_0) \frac{\partial^2 E(z, t)}{\partial t^2} = -j \frac{\omega}{2nc} \chi^{(3)} |E(z, t)|^2 E(z, t). \quad (2.19)$$

It is evident from the right hand side of Eq. (2.19) that the optical Kerr effect is a reactive process which produces an additional phase shift proportional to the optical intensity.

## 2.3 Optical Solitons

In a lossless medium with anomalous dispersion where  $\beta''(\omega_0) < 0$ , higher frequency components of an optical pulse trail lower frequency components. Thus, in a linear medium, the pulse will broaden indefinitely as it propagates. On the other hand, in a Kerr medium, self-phase modulation produces a positive chirp across the central portion of the pulse. It is possible to find a steady-state pulse shape where the amount of self-phase modulation balances the effect of dispersion exactly. The pulse then propagates undistorted in the form of an optical soliton.

To show that soliton solutions exist for Eq. (2.19), we first normalize the equation according to (see Appendix A for more details)

$$z_n = \frac{z - v_{\text{group}} t}{z_c} \quad (2.20)$$

$$t_n = \frac{t}{t_c} \quad (2.21)$$

$$u_n = \frac{E}{E_0} \quad (2.22)$$

and choose  $z_c$ ,  $t_c$ , and  $E_0$  such that both conditions

$$|\beta''(\omega_0)| \frac{z_c}{t_c^2} = 1 \quad (2.23)$$

and

$$\frac{\omega}{2nc} \chi^{(3)} E_0^2 z_c = 1 \quad (2.24)$$

are satisfied. The normalized nonlinear Schrödinger equation then takes a simple form

$$j \frac{\partial u_n}{\partial z_n} = \frac{1}{2} \frac{\partial^2 u_n}{\partial t_n^2} + |u_n|^2 u_n . \quad (2.25)$$

In 1972, Zakharov and Shabat [17] applied the technique of inverse scattering [18] to solve the above nonlinear partial differential equation. Their analytical solutions revealed that the amplitude and the velocity of interacting/colliding solitons did not change, whereas their phases contained discontinuities. The fundamental soliton is the simplest form of an extensive family of exact solutions of Eq. (2.25). It has an hyperbolic secant form

$$u(z_n, t_n) = \text{sech}(t_n) e^{-jz_n/2} . \quad (2.26)$$

## 2.4 Nonlinear Polarization Rotation

The principle of nonlinear polarization rotation [19] can be used to enhance the performance of a modelocked laser or a pulse storage ring. Mathematically, if

$$\mathbf{E}(t) = \hat{\mathbf{x}}E_x(t) + \hat{\mathbf{y}}E_y(t) \quad (2.27)$$

and we write each scalar component using a Fourier expansion,

$$E_x(t) = \frac{1}{2} [E_x(\omega)e^{-j\omega t} + E_x^*(\omega)e^{j\omega t}] , \quad (2.28)$$

we can rewrite the nonlinear part of polarization in Eq. (2.17) as

$$P_x^{\text{NL}}(\omega) = \frac{\epsilon_0 \chi^{(3)}}{4} [3 |E_x(\omega)|^2 E_x(\omega) + 2 |E_y(\omega)|^2 E_x(\omega) + E_y(\omega)^2 E_x^*(\omega)] . \quad (2.29)$$

A similar equation also holds for  $P_y(\omega)$ . In a circular polarization basis,

$$P_+^{\text{NL}}(\omega) = \frac{\epsilon_0 \chi^{(3)}}{2} [ |E_+(\omega)|^2 + 2 |E_-(\omega)|^2 ] E_+(\omega) , \quad (2.30)$$

$$P_-^{\text{NL}}(\omega) = \frac{\epsilon_0 \chi^{(3)}}{2} [ |E_-(\omega)|^2 + 2 |E_+(\omega)|^2 ] E_-(\omega) . \quad (2.31)$$

The above equations describe the evolution of two circular eigenmodes. If the polarization of the electric field is elliptical, the propagation constants of the two eigenmodes will be different, resulting in an intensity-dependent rotation of the total electric field.

Nonlinear polarization rotation can be used to produce an intensity dependent intracavity transmission. In Figure 2-2, the waveplate transforms a linearly polarized pulse into an elliptically polarized one, before it is launched into a Kerr medium such as an optical fiber. Because of the nonlinear intensity-dependent refractive index, the peak of the pulse will acquire more phase shift than will the wings of the pulse. The analyzer at the end of the fiber transforms this intensity-dependent rotation into amplitude modulation. This is known as the additive-pulse modelocking (APM) action. A typical plot of intracavity transmission vs. light intensity is shown in Figure 2-3. The transmission increases with increasing light intensity, peaks, and then decreases with further increase in intensity.

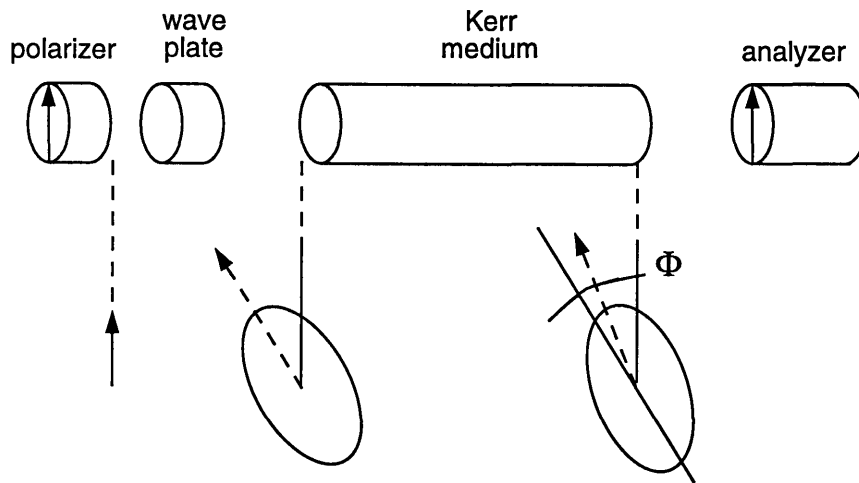


Figure 2-2: The additive-pulse modelocking action through nonlinear polarization rotation.

Other transmission vs. intensity responses can be obtained by changing the linear bias of the waveplates. For example, the slope of the transmission curve can be made negative so that low intensity light will experience preferential gain over high intensity light.

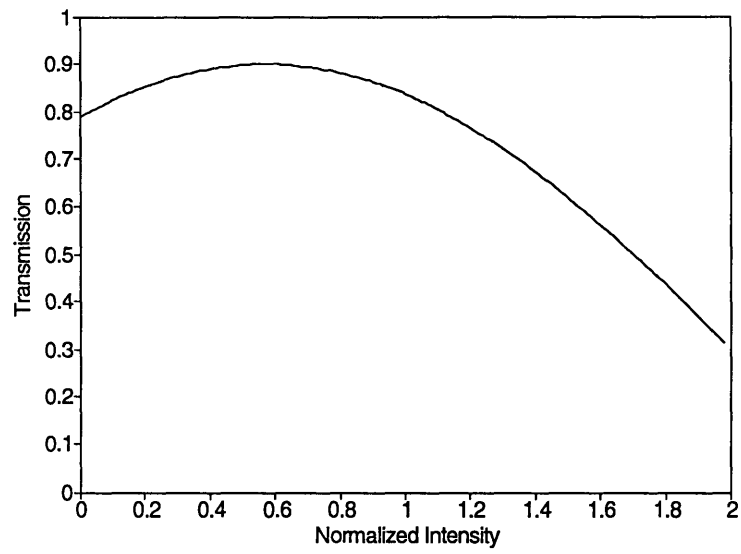


Figure 2-3: Plot of intracavity transmission vs. normalized intensity.

# Chapter 3

## Stability and Timing Maintenance in Soliton Transmission and Storage Rings

*This work was done with Dr. John D. Moores, who also wrote sections 3.1 and 3.3.1. It is published in [20].*

Pulse storage rings are potentially useful devices, e.g. for buffering data in optical communications networks. Perhaps the most successful storage ring demonstrated to date has been the synchronous recirculating loop of Nakazawa et al. [9, 21, 22] (intended as a long-distance transmission simulator, but clearly of use as a storage ring). Filtering [12, 23, 24] and amplitude modulation [13] were used in this loop to preserve the timing of the ONE's (solitons) and to suppress the growth of noise in bit intervals containing ZERO's (absence of solitons). Sliding-guiding filtering [25–27] improves the suppression of continuum, but may be less convenient for compact storage rings or in a network environment. More recently, analyses of the benefits of phase modulation have appeared [28–30]. Here, we propose the use of intensity-dependent absorption/gain (which we abbreviate FSA/G for fast saturable absorption/gain) to provide a thresholding effect which not only guarantees suppression of low intensities (robustness of ZEROs), but also provides a restoring force for intensity, driving the

intensity to a fixed value. This is not only beneficial for maintaining the intensity and width of the pulses, but also for reducing timing jitter, because the Raman self-frequency shift (RSFS) and third-order fiber dispersion (TOD) both couple intensity fluctuations into timing jitter. The most desired behavior, discussed in greater detail below, is FSG at low powers, FSA at intermediate powers, and FSG at high powers. We denote this combination of effects FSG+A+G. Much easier to implement, yet still quite suitable, is FSA+G (FSA at low powers, FSG at high powers), which we demonstrate via simulation. The intensity-dependent absorption may be provided by self-phase modulation followed by an interferometric transformation of phase modulation into amplitude modulation (as in Additive Pulse Mode-Locking [31]).

Regarding the analysis in this chapter, there are of course several effects which we have not considered, yet which limit transmission and storage. In pushing to very high bit rates, dispersive wave generation should not be overlooked, as it drains energy from the pulses, can be detected as false ONEs, and can induce timing jitter in the ONEs. Deleterious effects of polarization mode dispersion (PMD) are not discussed, as it is assumed that low PMD fibers and components are used. Also of importance are effects such as the phase-dependent soliton-soliton interaction, electrostriction, etc. We anticipate that the compensation schemes described below will reduce the impact of these effects as well. Furthermore, although our analysis assumes near-soliton ONE's, we anticipate the utility of these compensation schemes for other types of nonlinear ONE's.

### 3.1 Model

The starting equation includes effects of filters, modulators, and intensity-dependent absorption, so as to make it applicable to either storage rings or to long distance transmission.

The path-averaged nonlinear Schrödinger equation with (in order of appearance) noise, RSFS, TOD, extra gain required to balance filtering loss, four terms which are a polynomial fit to the intensity-dependent absorption/gain, amplitude modulation,

phase modulation, and filtering, can be written

$$\begin{aligned}
\frac{\partial u}{\partial z} &+ jD \frac{\partial^2 u}{\partial t^2} + jr^2 \delta |u|^2 u = S + jc_R r^2 \delta \frac{\partial |u|^2}{\partial t} u + \frac{k'''}{6} \frac{\partial^3 u}{\partial t^3} \\
&+ \Delta g u + (-L_{\text{FSA}} + \gamma_3 |u|^2 + \gamma_5 |u|^4 + \gamma_7 |u|^6) u \\
&- \frac{1}{2l_{\text{AM}}} M_{\text{AM}} \omega_{\text{AM}}^2 (t + T - T_{\text{AM}})^2 u + j \frac{1}{2l_{\text{PM}}} M_{\text{PM}} \omega_{\text{PM}}^2 (t + T - T_{\text{PM}})^2 u \\
&+ \frac{1}{l_f} \left\{ \left[ j\chi - \frac{\chi^2}{2} - j\frac{\chi^3}{3} \right] u + \frac{1}{\Omega_f} [-1 - j\chi + \chi^2] \frac{\partial u}{\partial t} \right. \\
&\left. + \frac{1}{\Omega_f^2} \left[ \frac{1}{2} + j\chi \right] \frac{\partial^2 u}{\partial t^2} + \frac{1}{\Omega_f^3} \left[ -\frac{1}{3} \right] \frac{\partial^3 u}{\partial t^3} \right\} \tag{3.1}
\end{aligned}$$

where

$$D = \frac{|k''|}{2} = \frac{1}{2} \left| \frac{\partial^2 k}{\partial \omega^2} \right|, \tag{3.2}$$

$$\delta = \frac{2\pi n_2 \hbar \omega_0}{\lambda_0 A_{\text{eff}}}, \tag{3.3}$$

$$\chi = \frac{p - \omega_{f0}}{\Omega_f}, \tag{3.4}$$

$k''$  and  $k'''$  represent path-averaged values, and  $c_R$  is the effective relaxation time associated with RSFS.

$A_{\text{eff}}$  is the modal effective area in the fiber,  $\hbar (= 1.05 \times 10^{-34} \text{ J}\cdot\text{s})$  is Planck's constant divided by  $2\pi$ ,  $\omega_0$  is the soliton initial carrier (mean) frequency (rad/s), and for silica the nonlinear index  $n_2 = 3.2 \times 10^{-20} \text{ m}^2/\text{W}$ . In the case of long-distance transmission, we should also average over the polarization scattering, which gives an extra factor of 8/9 on  $\delta$  [32]. We have normalized the field such that

$$n = \int_{-\infty}^{+\infty} |u|^2 dt \tag{3.5}$$

is the photon number. From path-averaging [33,34],

$$r^2 = (1 - e^{-2\Gamma l}) / (2\Gamma l) \tag{3.6}$$

where  $\Gamma$  is the field loss coefficient which accounts for fiber loss, splice losses, etc. but

not filter loss, and  $l$  is the distance between successive amplifiers. This factor applies to the self-Raman effect as well as the Kerr effect. The coefficient  $c_R$  is a measure of the strength of the RSFS term, which is a fraction of the Raman delay time, weighted by the shape of the Raman response curve. Path-averaging is valid if the amplifier spacing  $l$  is much less than the soliton phase period (which is eight times larger than  $z_0$ , the so-called soliton period)  $8z_0 = 2\pi\tau^2/D$ .

In the absence of filtering, the path-averaged gain should be zero. With filtering, solitons experience additional loss, which is compensated by excess gain  $\Delta g$ . The gain is a function of pump power, pulse energy, and the number of ONE's in the ring. It is clear that in the steady-state, the saturated level of gain is a major factor determining the number of pulses which can be stably supported. The dynamic saturation of the gain is an important consideration when the number of pulses in the loop changes. It is anticipated that in many systems, the dynamics of gain saturation will not be as important for dynamic stability as the compensation techniques discussed in this paper, because of the time scales. It is not our objective in this chapter to address the implications of dynamic gain saturation, and we take the gain and  $\Delta g$  to be fixed in the analysis.

The filtering terms we have chosen are for illustrative purposes. They are based upon the approximation of the logarithm of a complex Lorentzian for small deviations from the center frequency  $\Omega_f$  of the filter with filter length  $l_f$ . We have truncated the expansion at third order. At the next order, we would have picked up an imaginary third-derivative term which could help to cancel RSFS, but the imaginary first-derivative term already does so in the perturbative treatment.

We define several relevant frequencies and frequency shifts:  $\omega_0$  is the initial carrier frequency of the solitons,  $(\omega_0 - p)$  is the actual carrier frequency of a soliton, and  $\omega_{f0}$  is the difference between  $\omega_0$  and the filter center frequency. See Figure 3-1.

We define the timing of the initial soliton to be zero, the current timing of the soliton is  $T$ , and  $T_{PM}$  and  $T_{AM}$  are the timing of the phase and amplitude modulation.

Intensity-dependent absorption can be achieved in many ways. Examples include



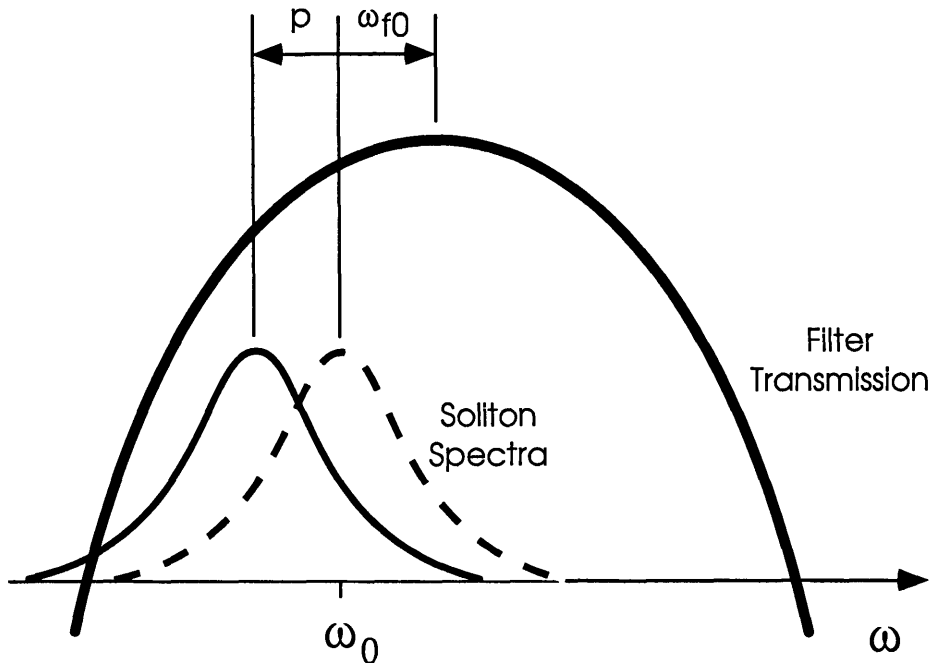


Figure 3-1:  $\omega_0$  is the initial carrier frequency of the solitons,  $(\omega_0 - p)$  is the actual carrier frequency of a soliton, and  $\omega_{f0}$  is the difference between  $\omega_0$  and the filter center frequency.

nonlinear Mach-Zender interferometers, asymmetric loop mirrors, and the use of nonlinear polarization ellipse rotation with polarizers and waveplates. These examples exhibit absorption which is an oscillatory function of intensity and which can be adequately approximated with a polynomial in intensity (simplifying the analysis). If the device is biased so that as the pulse intensity increases, the loss decreases (increases), the device imitates FSA (FSG). In the analysis (but not in the simulations), we treat the effect as distributed. If the pulse intensities are sufficiently high, the wings of the pulse can see FSA while the peak sees FSG (FSA+G), or vice-versa. Taken one step further, FSG+A+G in conjunction with gain, can be used to make a bistable storage ring with thresholding. Ideally we would bias the device so that very low intensities see loss, damping out noise and dispersive waves. Intermediate intensities see gain (which can be balanced e.g. by filtering). High intensities see decreasing gain with increasing intensity, which provides a restoring force for the peak intensity [35, 36]. A sample effective gain vs. intensity curve which incorporates FSG+A+G, and its cubic fit, are shown in Figure 3-2. For FSG+A+G, the polynomial coefficients satisfy

$L_{\text{FSA}}, \gamma_5 > 0$  and  $\gamma_3, \gamma_7 < 0$ , and for FSA+G,  $L_{\text{FSA}}, \gamma_3 > 0$ ,  $\gamma_5 < 0$ , and  $\gamma_7 = 0$ . It is anticipated that this thresholding will be beneficial with waveforms other than near-solitons, as well as near-solitons.

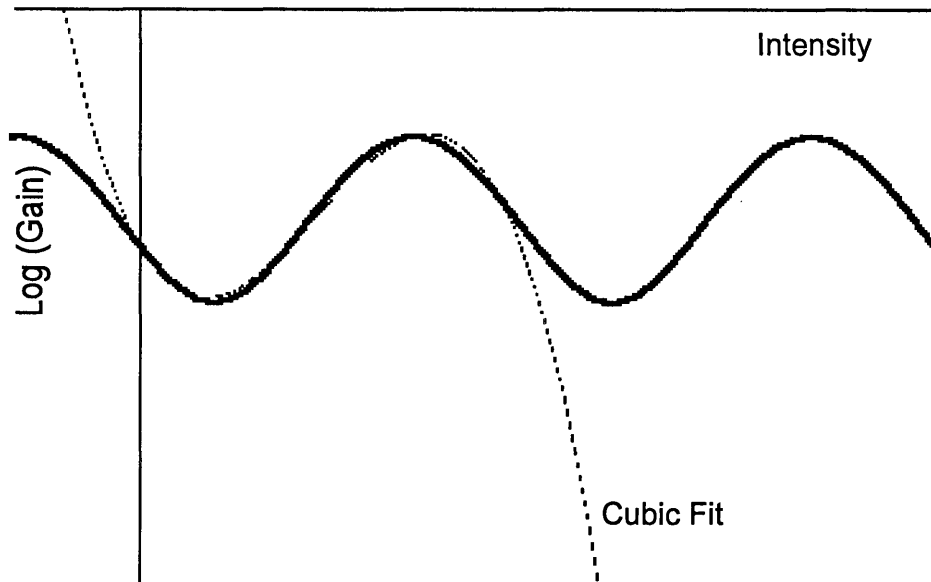


Figure 3-2: Cubic fit to effective gain vs. intensity with interferometric FSG+A+G.

The phase (amplitude) modulation in our model is completely described by a frequency of modulation  $\omega_{\text{PM}}(\omega_{\text{AM}})$ , timing  $T_{\text{PM}}(T_{\text{AM}})$ , and depth of modulation  $M_{\text{PM}}(M_{\text{AM}})$  per length  $l_{\text{PM}}(l_{\text{AM}})$ . The modulation frequency is likely to be  $2\pi/R$ , where  $R$  is the bit rate. We use a distributed model for the action of periodic lumped modulators. Suppose the lumped amplitude modulator multiplies the time profile by  $(1 - M_{\text{AM}} + M_{\text{AM}} \cos \omega_{\text{AM}} t)$ , where  $M_{\text{AM}}$  is actually half of the full depth of modulation. Then the corresponding distributed operator is  $(1/l_{\text{AM}}) \ln(1 - M_{\text{AM}} + M_{\text{AM}} \cos \omega_{\text{AM}} t)$ , which is approximately  $-M_{\text{AM}} \omega_{\text{AM}}^2 t^2 / (2l_{\text{AM}})$ . If the phase modulator multiplies the time profile by  $\exp -j\{\phi_{\text{PM}} + M_{\text{PM}}(\cos \omega_{\text{PM}} t - 1)\}$ , then the corresponding distributed operator is  $(-j/l_{\text{PM}})\{\phi_{\text{PM}} + M_{\text{PM}}(\cos \omega_{\text{PM}} t - 1)\}$ , or approximately  $-M_{\text{PM}} \omega_{\text{PM}}^2 t^2 / (2l_{\text{PM}})$ , where we have ignored the constant phase term which can be trivially scaled out. The obvious implementation is with discrete electro-optic modulators. However, it may be possible to achieve continuous phase modulation using cross-phase modulation, as we discuss elsewhere.

The term  $S$  represents both the noise introduced by the amplifiers and the noise

from zero-point fluctuations due to the loss. It is assumed that the gain balances the loss. Strictly, the noise and the soliton amplitude should be treated as operators. In a quantum analysis, half of the noise is due to the zero-point fluctuations associated with the loss, and half with those associated with the gain (when the gain medium is distributed and perfectly inverted). A semiclassical analysis gives the same result, if the total noise is associated with the compensation by the amplifiers of the loss. In the limit of distributed amplification, with white, delta-function-correlated noise we have [33]

$$\langle S^*(t_1, z_1)S(t_2, z_2) \rangle = \frac{\beta(G-1)}{l} \delta(z_1 - z_2) \delta(t_1 - t_2), \quad (3.7)$$

where  $\beta$  is the excess noise parameter [37],  $G$  is the power gain of an amplifier, and  $l$  is the distance between amplifiers. We have normalized  $|u^2|$  to photon flux (photon number per unit time), which accounts for the absence of the factor  $\hbar\omega_0$  in (3.7).

If the communication system or memory device is such that the gain is not distributed to cancel the loss at each point, but the gain is lumped into amplifiers, it has been shown [33, 34] that soliton behavior can be maintained on the average under practically realizable conditions. There is a path-averaging noise-penalty factor [33, 37]

$$f = \frac{(G-1)^2}{G \ln^2 G} \quad (3.8)$$

which will arise in our analysis. The gain balances the loss, or  $2\Gamma l = \ln G$ , where  $l$  is the distance between amplifiers. The path-averaging factor  $r^2$  (see Eq. (3.6)) therefore satisfies

$$r^2 = \frac{(G-1)}{G \ln G}. \quad (3.9)$$

Effectively,

$$\langle S^*(t_1, z_1)S(t_2, z_2) \rangle = N_N \delta(z_1 - z_2) \delta(t_1 - t_2) \quad (3.10)$$

where

$$N_N = \frac{2\Gamma\beta f}{r^2}. \quad (3.11)$$

For example, with  $\Gamma = 0.0242 \text{ km}^{-1}$  (power loss of 0.21 dB/km) and  $l = 20 \text{ km}$ , we find that  $f = 1.081$  and  $r^2 = 0.64$ . For a storage ring of length  $l = 1 \text{ km}$ , the noise

penalty and path-averaging coefficient are close to unity:  $f = 1.0002$  and  $r^2 = 0.98$ .

## 3.2 Stability of Zeros

To analyze the stability of the ZEROs, we ignore the nonlinear and the TOD terms in Eq. (3.1), and focus on the spectral components of the noise near the passband of the filter where the detuning  $\chi \approx 0$ . We shall determine the conditions under which all eigenmodes of the linear evolution equation are damped.

The equation of motion for low intensity light (well below the intensity of a data pulse) is

$$\begin{aligned} \frac{\partial u}{\partial z} = & S - jD \frac{\partial^2 u}{\partial t^2} + \Delta g u - L_{\text{FSA}} u \\ & - \frac{1}{2l_{\text{AM}}} M_{\text{AM}} \omega_{\text{AM}}^2 t^2 u + j \frac{1}{2l_{\text{PM}}} M_{\text{PM}} \omega_{\text{PM}}^2 t^2 u \\ & + \frac{1}{2\Omega_f^2 l_f} \frac{\partial^2 u}{\partial t^2}. \end{aligned} \quad (3.12)$$

Following the approach by Haus and Mecozzi [11] we look for an eigenfunction solution to Eq. (3.12) of the form  $u_n(z, t) = Z_n(z)T_n(t)$ . Substitution of  $u_n(z, t)$  yields

$$\left( \frac{1}{2\Omega_f^2 l_f} - jD \right) \frac{d^2 T_n(t)}{dt^2} - \left( \frac{1}{2l_{\text{AM}}} M_{\text{AM}} \omega_{\text{AM}}^2 t^2 - j \frac{1}{2l_{\text{PM}}} M_{\text{PM}} \omega_{\text{PM}}^2 t^2 \right) T_n(t) = E_n T_n(t) \quad (3.13)$$

and

$$\frac{dZ_n(z)}{dz} = (\Delta g - L_{\text{FSA}} + E_n) Z_n(z) + S_n(z) \quad (3.14)$$

If we denote

$$\frac{1}{\tau_0^2} = \left[ \frac{\frac{M_{\text{AM}} \omega_{\text{AM}}^2}{l_{\text{AM}}} - j \frac{M_{\text{PM}} \omega_{\text{PM}}^2}{l_{\text{PM}}}}{\frac{1}{\Omega_f^2 l_f} - j2D} \right]^{\frac{1}{2}}, \quad (3.15)$$

the eigenfunctions

$$T_n(t) = \mathcal{H}_n \left( \frac{t}{\tau_0} \right) \exp \left( -\frac{t^2}{2\tau_0^2} \right) \quad (3.16)$$

are Hermite-Gaussian functions where

$$\mathcal{H}_n(t) = \sum_{m=0}^{n/2} \frac{(-1)^m n! (2t)^{n-2m}}{m!(n-2m)!} \text{ for } n=0, 1, 2, \dots$$

The eigenvalues are

$$E_n = -(2n+1) \left[ \left( \frac{1}{2l_{\text{AM}}} M_{\text{AM}} \omega_{\text{AM}}^2 - j \frac{1}{2l_{\text{PM}}} M_{\text{PM}} \omega_{\text{PM}}^2 \right) \left( \frac{1}{2\Omega_f^2 l_f} - jD \right) \right]^{\frac{1}{2}}. \quad (3.17)$$

There are two criteria to ensure the stability of the ZEROs. Firstly, the evolution of the low-intensity noise is damped provided that all its eigenmodes are damped:

$$\Delta g - L_{\text{FSA}} + \text{Re}[E_n] < 0 \quad (3.18)$$

for all  $n$ .

The value of  $\Delta g$  is chosen such that there is no systematic change in the photon number. From Eq. (3.32),

$$\Delta g = \frac{1}{6l_f \Omega_f^2 \tau^2} + \frac{\pi^2 \tau^2}{24l_{\text{AM}}} M_{\text{AM}} \omega_{\text{AM}}^2 + L_{\text{FSA}} - \frac{\gamma_3 n_o}{6\tau} - \frac{\gamma_5 n_o^2}{15\tau^2} - \frac{\gamma_7 n_o^3}{35\tau^3}. \quad (3.19)$$

The sequence  $\{\text{Re}[E_0], \text{Re}[E_1], \dots\}$  is monotonically decreasing. Therefore, one only needs to ensure that  $\Delta g - L_{\text{FSA}} + \text{Re}[E_0] < 0$  for stability. Since one can choose the parameters  $L_{\text{FSA}}$ ,  $\gamma_3$ ,  $\gamma_5$ , and  $\gamma_7$  freely in Eq. (3.19) to satisfy the first criterion, it is immediately clear that fast saturable absorption can suppress the growth of noise.

Secondly, the evolution of the change in the photon number in Eq. (3.33) has to be damped as well. This additional constraint is

$$-\frac{2}{3l_f \Omega_f^2 \tau^2} + \frac{\pi^2 \tau^2}{6l_{\text{AM}}} M_{\text{AM}} \omega_{\text{AM}}^2 + \frac{2\gamma_3 n_o}{3\tau} + \frac{8\gamma_5 n_o^2}{15\tau^2} + \frac{12\gamma_7 n_o^3}{35\tau^3} < 0 \quad (3.20)$$

Because it is not clear how to implement FSA/G in a long-haul, non-polarization-preserving transmission system, we shall analyze the stability of ZEROs in a system

without FSA/G. It is useful to define dimensionless variables

$$\begin{aligned}
 F &= \frac{\tau^2}{D} \frac{1}{l_f \Omega_f^2 \tau^2} \\
 \mu_{\text{AM}} &= \frac{\tau^2}{D} \frac{M_{\text{AM}} \omega_{\text{AM}}^2 \tau^2}{l_{\text{AM}}} \\
 \mu_{\text{PM}} &= \frac{\tau^2}{D} \frac{M_{\text{PM}} \omega_{\text{PM}}^2 \tau^2}{l_{\text{PM}}}
 \end{aligned}$$

that are proportional to the strength of filtering, amplitude modulation, and phase modulation, respectively.

### 3.2.1 Systems with Amplitude Modulation and Filtering

This case was also discussed by Haus and Mecozzi [11]. Without saturable absorption, the gain  $\Delta g$  must be kept below an upper limit set by Eq. (3.18). In terms of dimensionless variables,

$$\frac{F}{6} + \frac{\pi^2}{24} \mu_{\text{AM}} < \left( \frac{\mu_{\text{AM}}}{2} \right)^{\frac{1}{2}} \left[ \left( \frac{F}{2} \right)^2 + 1 \right]^{\frac{1}{4}} \cos \left[ \frac{1}{2} \tan^{-1} \left( \frac{2}{F} \right) \right]. \quad (3.21)$$

This inequality states that one cannot increase the filtering strength  $F$  arbitrarily.

The use of amplitude modulation tends to shorten the soliton pulse width and broaden its spectrum, which can be counteracted by filtering only if the amount of modulation is not excessive. Specifically, from Eq. (3.20), we require that

$$\frac{\pi^2}{24} \mu_{\text{AM}} < \frac{2}{3} F. \quad (3.22)$$

The stability region, bounded by Eq. (3.21) and Eq. (3.22), is shown in Figure 3-3.

### 3.2.2 Systems with Phase Modulation and Filtering

A phase modulator changes the phase of an input signal while leaving its photon number intact. Therefore, in the absence of amplitude modulation and saturable absorption, the criterion for photon number stability given by Eq. (3.20) is always

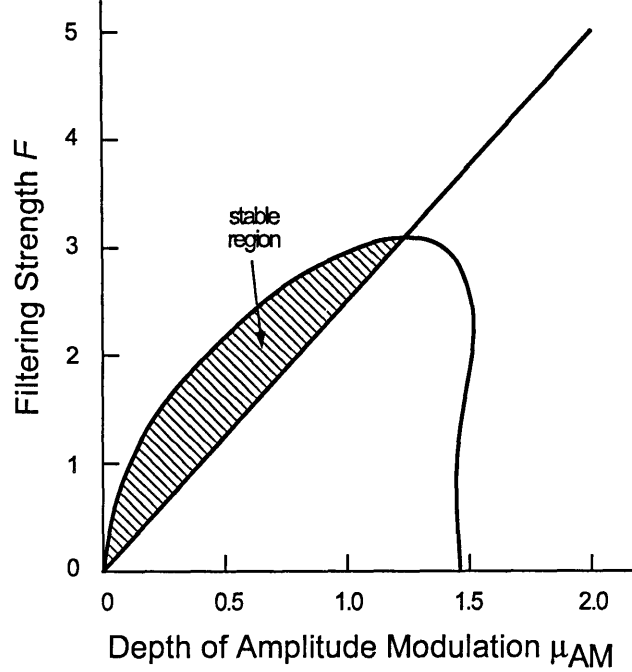


Figure 3-3: Theoretical stability diagram for soliton storage ring with amplitude modulation and filtering.

satisfied provided  $F > 0$ . The stability region is (see Figure 3-4):

$$\frac{F}{6} < \left(\frac{\mu\text{PM}}{2}\right)^{\frac{1}{2}} \left[\left(\frac{F}{2}\right)^2 + 1\right]^{\frac{1}{4}} \cos \left[\frac{1}{2} \tan^{-1} \left(\frac{F}{2}\right)\right]. \quad (3.23)$$

### 3.3 The ONEs

We consider classical and noise effects upon near-soliton pulses, using soliton perturbation theory.

#### 3.3.1 Soliton Perturbation Theory

A simple fundamental soliton solution of the unperturbed nonlinear Schrödinger equation (Eq. (3.1) without the RHS), is

$$u_0 = A_0 \operatorname{sech} \left\{ \frac{(t - T - 2Dpz)}{\tau} \right\} \exp j \left\{ -\frac{D}{\tau^2} z + Dp^2 z - p(t - T) + \theta \right\}. \quad (3.24)$$

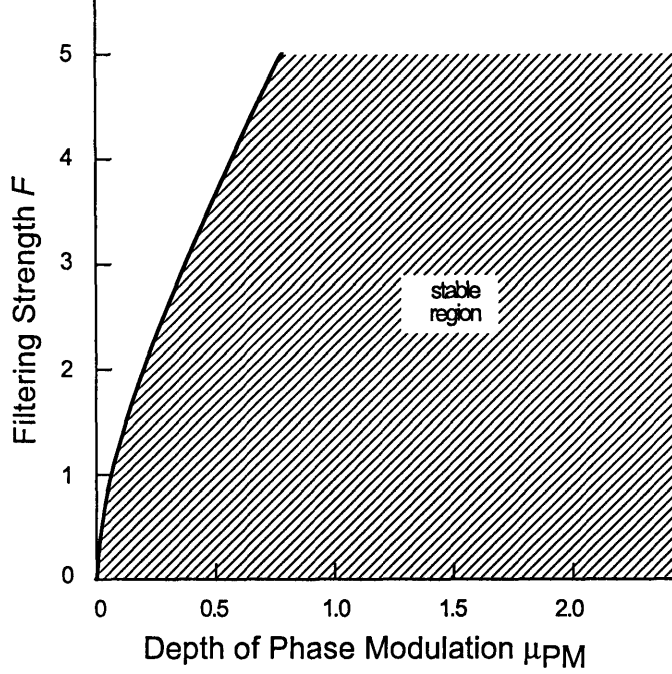


Figure 3-4: Theoretical stability diagram for soliton storage ring with phase modulation and filtering. Note that the system is marginally stable with no filtering (along the horizontal axis).

with  $\theta$  an arbitrary phase,  $T$  the temporal displacement,  $p$  the change of inverse group velocity, which is equivalent to the shift of frequency as defined above, and which we have labeled ' $p$ ' suggestive of quantum mechanical momentum [38]. Note that in this momentum analog, a positive momentum leads to motion in the positive  $t$  direction. However, this is a delay, and we are in the anomalous dispersion regime, where lower frequencies are delayed. Thus a positive change in momentum corresponds to a negative change in frequency. The pulsewidth

$$\tau = \left( \frac{4D}{nr^2\delta} \right) = 0.567\tau_{\text{FWHM}} \quad (3.25)$$

where  $\tau_{\text{FWHM}}$  is full-width-at-half-maximum-intensity, and

$$2A_0^2\tau = n. \quad (3.26)$$

The perturbation of a soliton may be treated as a perturbation of the photon



number  $\Delta n$ , displacement  $\Delta T$ , momentum  $\Delta p$ , and phase  $\Delta\theta$ . We can express this as [38]

$$\Delta u(z, t) = f_n(t)\Delta n(z) + f_T(t)\Delta T(z) + f_p(t)\Delta p(z) + f_\theta(t)\Delta\theta(z) + \text{continuum}. \quad (3.27)$$

By ‘continuum,’ we mean nonsoliton, dispersive wave radiation [17]. One can use the perturbation approach of Haus et al. [13,38] or equivalently, the approach of Kaup [39] with the pulse amplitude and width coupled.

Our approach will be to expand the driving terms (RHS of Eq. (3.1)) to first order in the soliton parameters, and to solve self-consistently. The continuum plays an important role if, for example, the TOD is sufficiently large, if the soliton period is too short, or if narrowband filters with fixed passband are used without saturable gain/absorption. Proper treatment of the continuum could also describe the long-term instability of RSFS and filtering simulated by Blow et al. [40]. The analysis in this section assumes that the influence of the continuum is weak. The parameters of the initial soliton are denoted with ‘0’ subscripts, and without loss of generality, we choose  $p=T=\theta=0$  at  $z = 0$ .

The ansatz (3.27) is introduced into (3.1) and the equations for  $\Delta n$ ,  $\Delta p$ ,  $\Delta T$  and  $\Delta\theta$  are projected out. The projection functions are the adjoints  $\underline{f}_i(t)$ , obeying the orthogonality relations [38]

$$\text{Re} \int_{-\infty}^{+\infty} \underline{f}_i^*(t) f_j(t) dt = \delta_{ij} \quad ; i, j \in \{n, T, p, \theta\} \quad (3.28)$$

and equal to

$$\begin{aligned} \underline{f}_n(t) &= 2A_0 \text{sech} \left( \frac{t}{\tau} \right) \\ \underline{f}_\theta(t) &= \frac{2j}{n} \left\{ 1 - \left( \frac{t}{\tau} \right) \tanh \left( \frac{t}{\tau} \right) \right\} A_0 \text{sech} \left( \frac{t}{\tau} \right) \\ \underline{f}_p(t) &= -\frac{2j}{n\tau} \tanh \left( \frac{t}{\tau} \right) A_0 \text{sech} \left( \frac{t}{\tau} \right) \\ \underline{f}_T(t) &= \frac{2}{n} t A_0 \text{sech} \left( \frac{t}{\tau} \right). \end{aligned}$$

We are not interested in the change of phase  $\theta$  (it does not couple back to the other parameters). We are interested in change of the soliton position (timing)  $\Delta T$  due to the fluctuations. The evolution equations of interest have many terms, but all have simple physical interpretation. They are at first presented in full, and then simpler limiting cases will be analyzed, culminating in an analysis of the entire system. The equations are:

$$\begin{aligned}
\frac{d\Delta n}{dz} = & \left[ 2\Delta g - \frac{1}{3l_f\Omega_f^2\tau^2} - \frac{\omega_{f0}^2}{l_f\Omega_f^2} - \frac{\pi^2\tau^2}{12l_{AM}}M_{AM}\omega_{AM}^2 - \frac{M_{AM}\omega_{AM}^2T_{AM}^2}{l_{AM}} \right. \\
& + \left. \left( -2L_{FSA} + \frac{\gamma_3 n_o}{3\tau} + \frac{2\gamma_5 n_o^2}{15\tau^2} + \frac{2\gamma_7 n_o^3}{35\tau^3} \right) \right] n_o \\
& + \left[ 2\Delta g - \frac{1}{l_f\Omega_f^2\tau^2} - \frac{\omega_{f0}^2}{l_f\Omega_f^2} + \frac{\pi^2\tau^2}{12l_{AM}}M_{AM}\omega_{AM}^2 - \frac{M_{AM}\omega_{AM}^2T_{AM}^2}{l_{AM}} \right. \\
& + \left. \left( -2L_{FSA} + 3\frac{\gamma_3 n_o}{3\tau} + 5\frac{2\gamma_5 n_o^2}{15\tau^2} + 7\frac{2\gamma_7 n_o^3}{35\tau^3} \right) \right] \Delta n \\
& + \left( \frac{2n_o\omega_{f0}}{l_f\Omega_f^2} \right) \Delta p + \frac{2M_{AM}\omega_{AM}^2T_{AM}}{l_{AM}}\Delta T + S_n(z) \tag{3.29}
\end{aligned}$$

$$\begin{aligned}
\frac{d\Delta p}{dz} = & \left( \frac{16c_{RD}}{15\tau^4} + \frac{2\omega_{f0}}{3l_f\Omega_f^2\tau^2} + \frac{M_{PM}\omega_{PM}^2T_{PM}}{l_{PM}} \right) \\
& + \left( \frac{64c_{RD}}{15\tau^4 n_o} + \frac{4\omega_{f0}}{3l_f\Omega_f^2\tau^2 n_o} \right) \Delta n - \left( \frac{2}{3\tau^2 l_f\Omega_f^2} \right) \Delta p \\
& - \frac{M_{PM}\omega_{PM}^2}{l_{PM}}\Delta T + S_p(z) \tag{3.30}
\end{aligned}$$

$$\begin{aligned}
\frac{d\Delta T}{dz} = & \left( \frac{k'''}{6\tau^2} + \frac{\pi^2\tau^2 M_{AM}\omega_{AM}^2 T_{AM}}{6l_{AM}} + \frac{1}{l_f\Omega_f} - \frac{\omega_{f0}^2}{l_f\Omega_f^3} - \frac{1}{3l_f\Omega_f^3\tau^2} \right) \\
& + \left( \frac{k'''}{3\tau^2 n_o} - \frac{\pi^2\tau^2 M_{AM}\omega_{AM}^2 T_{AM}}{3n_o l_{AM}} - \frac{2}{3l_f\Omega_f^3\tau^2 n_o} \right) \Delta n \\
& + \left( 2D + \frac{2\omega_{f0}}{l_f\Omega_f^3} \right) \Delta p - \frac{\pi^2\tau^2 M_{AM}\omega_{AM}^2}{6l_{AM}}\Delta T + S_T(z). \tag{3.31}
\end{aligned}$$

In the equation for  $\Delta n$ , Eq. (3.29), there is excess gain required to offset the loss seen by the pulse from filtering and amplitude modulation. There is filtering loss from the finite bandwidth of the pulse and more loss if the pulse carrier frequency

is offset from the center of the filter passband. The amplitude modulator gives loss as a function of timing, so a wider pulse will see more loss. Furthermore, if the pulse is offset from the timing of the modulator, there will be loss. The final four terms multiplying  $n_o$  are the FSA/G terms, which by definition provide loss that is a function of intensity. Next we have a large number of terms multiplying  $\Delta n$ . The interpretation of these is the same as for the terms multiplying  $n_o$ , but these terms show the trends as the photon number changes. Most have the same sign, with one exception - the amplitude modulator term which depends on the pulse width. This simply means that there is net loss due to AM, and the loss increases as the pulse gets weaker and wider. The term multiplying  $\Delta p$  shows that as the pulse carrier frequency shifts, the pulse sees more or less loss depending upon whether the carrier frequency is moving away from or towards the center of the filter passband. The  $\Delta T$  term is similar, showing that as the pulse drifts in time, it sees more or less loss as it moves away from or towards the timing of maximum transmission through the amplitude modulator. The final term is that portion of the noise which affects the photon number of the pulse.

The gain of the fiber amplifiers has to be adjusted so that there is no systematic change of the photon number, i.e.

$$\begin{aligned}
2\Delta g &= \frac{1}{3l_f\Omega_f^2\tau^2} + \frac{\omega_{f0}^2}{l_f\Omega_f^2} + \frac{\pi^2\tau^2}{12l_{AM}}M_{AM}\omega_{AM}^2 + \frac{M_{AM}\omega_{AM}^2T_{AM}^2}{l_{AM}} \\
&+ 2L_{FSA} - \frac{\gamma_3 n_o}{3\tau} - \frac{2\gamma_5 n_o^2}{15\tau^2} - \frac{2\gamma_7 n_o^3}{35\tau^3}.
\end{aligned} \tag{3.32}$$

The equation for  $\Delta n$  then simplifies:

$$\begin{aligned}
\frac{d\Delta n}{dz} &= \left[ -\frac{2}{3l_f\Omega_f^2\tau^2} + \frac{\pi^2\tau^2}{6l_{AM}}M_{AM}\omega_{AM}^2 + \left( \frac{2\gamma_3 n_o}{3\tau} + \frac{8\gamma_5 n_o^2}{15\tau^2} + \frac{12\gamma_7 n_o^3}{35\tau^3} \right) \right] \Delta n \\
&+ \left( \frac{2n_o\omega_{f0}}{l_f\Omega_f^2} \right) \Delta p + \left( \frac{2M_{AM}\omega_{AM}^2T_{AM}}{l_{AM}} \right) \Delta T + S_n(z)
\end{aligned} \tag{3.33}$$

At least naively, the larger the quantity  $(\Delta g - L_{FSA})$ , the greater is the opportunity for the growth of noise at the center frequency of the filter and at the maximum

transmission of the amplitude modulator. In a memory device, it should be possible to keep  $(\Delta g - L_{\text{FSA}}) < 0$ , suppressing the growth of noise. By simply choosing parameters such that the peak intensity of the pulse sees sufficient loss with increasing intensity from the FSA/G, the sum of the FSA/G terms with  $\gamma$ -coefficients in Eq. (3.33) will be negative. Cases with no saturable absorption/gain are treated in Section IV.

In the equation for  $\Delta p$ , Eq. (3.30), the first  $c_R$  term is the classical self-frequency shift. The next term is frequency-pulling (from the effective refractive index profile associated with the filter) due to the initial offset of center frequencies. The third term is frequency-pulling from the phase modulator, which chirps mistimed pulses. At the next order, we have the terms multiplying  $\Delta n$ . The first shows that if the photon number fluctuates, then the power and bandwidth of the soliton change, and this alters the rate of RSFS - increased photon number (intensity and bandwidth) implies stronger RSFS. The other term shows that as the pulse bandwidth changes, the frequency pulling due to the filtering changes. The  $\Delta p$  term describes the restoring force which filtering imposes on the pulse center frequency. The  $\Delta T$  term shows that as the pulse walks off in time, it is chirped by the phase modulator. Finally, there is the noise  $S_p$ .

The lowest order terms in Eq. (3.31) are the deterministic timing terms, which, if we are interested in timing jitter only, can be ignored. Briefly, these terms show that larger pulse bandwidths lead to timing shifts via TOD, offset amplitude modulation pulls the timing, the reactive nature of the filtering changes the group spatial velocity directly and also acts like TOD. Next we have three terms by which changes in photon number affect timing. The first says that as the bandwidth changes, TOD changes the group velocity. The second says that if the pulse is offset from the timing of the amplitude modulator, then there is pulling in time, and the strength of the pulling depends on the pulse width. The third is just like the first, except that the filter provides the TOD. The terms multiplying  $\Delta p$  are simply group velocity dispersion terms, one from fiber dispersion, and the other from the dispersive nature of the filtering. The  $\Delta T$  term shows that amplitude modulation provides a restoring force

for timing. The last term is timing noise.

The noise sources  $S_i(z)$  are the projections

$$S_i(z) = \text{Re} \int_{-\infty}^{+\infty} \underline{f}_i^*(t) S(t, z) dt . \quad (3.34)$$

Now that we have obtained the general equations of motion, let us restrict our attention to some specific cases. First we shall consider the uncompensated case, in which RSFS, TOD, and noise-induced jitter go unchecked. We shall find that the growth rate of the soliton timing fluctuations about the deterministic (shifting) position can be greater than the growth rate for Gordon-Haus fluctuations. The second case of interest is that in which filtering is chosen to preserve the classical (i.e. lowest order, deterministic) photon number, and to cancel the classical RSFS. We assume weak RSFS or closely-spaced filters for RSFS cancellation. At higher bit rates, it may be necessary to downshift the filters with distance, in accordance with the classical RSFS, so that the frequency of a channel as received will be lower than the frequency transmitted.

### 3.3.2 Evolution of Uncompensated Systems

#### 3.3.2.1 Classical

In the absence of noise, the soliton parameters evolve according to

$$\frac{d\Delta n}{dz} = 0 \quad (3.35)$$

$$\frac{d\Delta p}{dz} = \left( \frac{16c_R D}{15\tau^4} \right) + \left( \frac{64c_R D}{15\tau^4 n_0} \right) \Delta n \quad (3.36)$$

$$\frac{d\Delta T}{dz} = \left( \frac{k'''}{6\tau^2} \right) + \left( \frac{k'''}{3\tau^2 n_0} \right) \Delta n + 2D\Delta p . \quad (3.37)$$

Solving the above linear system of ODEs, assuming  $\Delta n(0) = 0$  yields

$$\Delta n(z) = 0 \quad (3.38)$$

$$\Delta p(z) = \Delta p(0) + \frac{16c_R D}{15\tau^4} z \quad (3.39)$$

$$\Delta T(z) = \Delta T(0) + \frac{k'''}{6\tau^2}z + 2D\Delta p(0)z + \frac{16c_R D}{15\tau^4}z^2. \quad (3.40)$$

The linear growth in timing delay is due to both TOD and detuning in frequency, while the quadratic growth in timing delay is due to the RSFS. In order to store pulses permanently in a ring at steady-state, one needs to combat these classical (deterministic) timing delays. Otherwise, the frequency of the solitons will be red-shifted continuously until it is counteracted by the gain bandwidth of the optical amplifier.

### 3.3.2.2 Stochastic

Solution of the equations of motion in the presence of noise is simplified by unilaterally Laplace transforming in  $z$ . We label the transform variable  $s$  (to compare with Ref. [13], we can write  $s = \text{Re } s - jK$ ).

We define the autocorrelation with respect to the value at  $z = 0$ . In the evaluation of noise projections we use

$$\int_{-\infty}^{+\infty} dt \langle S^*(t, z)S(t', 0) \rangle = N_N \delta(z), \quad (3.41)$$

and thus

$$\mathcal{L} \left\{ \int_{-\infty}^{+\infty} dt \langle S^*(t, z)S(t', 0) \rangle \right\} = N_N \quad (3.42)$$

where  $\mathcal{L}$  indicates unilateral spatial Laplace transformation. Evaluating the projections, we find

$$\langle S_p^*(s)S_p(s) \rangle = \left( \frac{4}{3n_0\tau^2} \right) N_N \quad (3.43)$$

$$\langle S_n^*(s)S_n(s) \rangle = 4n_0 N_N \quad (3.44)$$

$$\langle S_T^*(s)S_T(s) \rangle = \left( \frac{\pi^2\tau^2}{6n_0} \right) N_N. \quad (3.45)$$

Henceforth we adopt the notational simplification  $\langle S_j^*(s)S_j(s) \rangle \rightarrow \langle S_j^2 \rangle$ ,  $j = n, p, T$ .

Without compensation, the equations of motion are greatly simplified:

$$\frac{d\Delta n}{dz} = S_n(z) \quad (3.46)$$

$$\frac{d\Delta p}{dz} = \left(\frac{16c_R D}{15\tau^4} e\right) + \left(\frac{64c_R D}{15\tau^4 n_0}\right) \Delta n + S_p(z) \quad (3.47)$$

$$\frac{d\Delta T}{dz} = \left(\frac{k'''}{6\tau^2}\right) + \left(\frac{k'''}{3\tau^2 n_0}\right) \Delta n + 2D\Delta p + S_T(z). \quad (3.48)$$

Laplace transforming and solving, we find

$$\begin{aligned} \langle \Delta T^2 \rangle &= \frac{2^{10} c_R^2 D^2 \delta^2 r^4 \langle S_n^2 \rangle}{225 \tau^6 s^6} + \frac{2^4 c_R k''' \delta^2 r^4 \langle S_n^2 \rangle}{45 \tau^4 s^5} \\ &+ \frac{k'''' \delta^2 r^4 \langle S_n^2 \rangle}{144 D^2 \tau^2 s^4} + 4D^2 \frac{\langle S_p^2 \rangle}{s^4} + \frac{\langle S_T^2 \rangle}{s^2}. \end{aligned} \quad (3.49)$$

The first term is due to the photon number noise affecting RSFS. The second term is the effect of photon number noise on RSFS and TOD. The third term is due to photon number noise affecting pulse group velocity via TOD alone. The second term can be negative if  $k'''$  is negative, but of course the sum of the first three terms is positive semidefinite. The fourth term is noise associated with the Gordon-Haus effect. The fifth term is due to timing noise. Noting the Laplace transform pairs

$$\frac{1}{s^{m+1}} \longleftrightarrow \frac{z^m}{m!} \quad (3.50)$$

we immediately see the  $z^3$  growth of Gordon-Haus jitter and we see that RSFS can lead to  $z^5$  growth of jitter.

If one neglects TOD, the dominant terms in the timing variance are, typically, Raman jitter at large distances, Gordon-Haus jitter at intermediate distances, and direct timing jitter at very short distances. Performing the inverse Laplace transform of Eq. (3.49), the corresponding normalized timing variances are

$$\frac{\langle \Delta T(z)^2 \rangle_{\text{RSFS}}}{\tau^2} = \frac{2^{10} c_R^2 D^2 \delta^2 r^4 \langle S_n^2 \rangle z^5}{225 \tau^8 5!} = 3.5 \times 10^{-11} \left(\frac{z}{z_0}\right)^5 \frac{\tau_{\text{ps}}}{D'^2_{\text{ps/nm/km}}} \quad (3.51)$$

$$\frac{\langle \Delta T(z)^2 \rangle_{\text{GH}}}{\tau^2} = \frac{4D^2}{\tau^2} \langle S_p^2 \rangle \frac{z^3}{3!} = 1.1 \times 10^{-6} \left( \frac{z}{z_0} \right)^3 \frac{\tau_{\text{ps}}^3}{D'^2_{\text{ps/nm/km}}}, \quad (3.52)$$

$$\frac{\langle \Delta T(z)^2 \rangle_{\text{T}}}{\tau^2} = \frac{1}{\tau^2} \langle S_T^2 \rangle z = 3.2 \times 10^{-6} \left( \frac{z}{z_0} \right) \frac{\tau_{\text{ps}}^3}{D'^2_{\text{ps/nm/km}}}. \quad (3.53)$$

The expressions at the far right assume that the parameters of our system are  $c_R = 2.5$  fs,  $\delta = 4.7 \times 10^{-22}$  s/m, noise figure  $\beta = 2.0$ , loss = 0.204 dB/roundtrip, and the loop length is 2 m.

Although the proportionality constant for the RSFS-induced timing variance is five orders of magnitude smaller than that of the Gordon-Haus jitter, the RSFS-induced timing variance varies linearly with pulse width, whereas the normalized Gordon-Haus jitter varies as the cubic power of pulse width. As bit rates increase (or  $\tau$  decreases), RSFS jitter quickly gains prominence. Furthermore, RSFS jitter grows much faster with distance than Gordon-Haus jitter. In order to observe, in numerical simulations, the transition from Gordon-Haus-dominated jitter to RSFS-dominated jitter without using excessive CPU time, we simulated pulses of 0.1 ps FWHM. Specifically, a single pulse was propagated in a storage ring with noise added at each amplifier stage. The dispersion was  $D' = 0.5$  ps/nm/km. Single pulses were used to ensure that the soliton-soliton interaction imparted no jitter. Using an ensemble of 25 runs, the trajectories were then compared with an ideal noiseless trajectory to obtain the timing variance. The agreement between theory and the simulation results is fairly good. The results are shown in Figure 3-5. The solid curve is the numerical variance, and the dashed curve is the prediction from perturbation theory. Note that the curve changes its slope from +3 to +5 at approximately  $z = 20z_0$ , which in this example is approximately 16 km.

### 3.3.3 Evolution of Systems Compensated with Phase Modulation and Filtering

It is important to maintain an optical pulse pattern of ONEs and ZEROs against noise and high-order effects. In this section, a method using phase modulation and



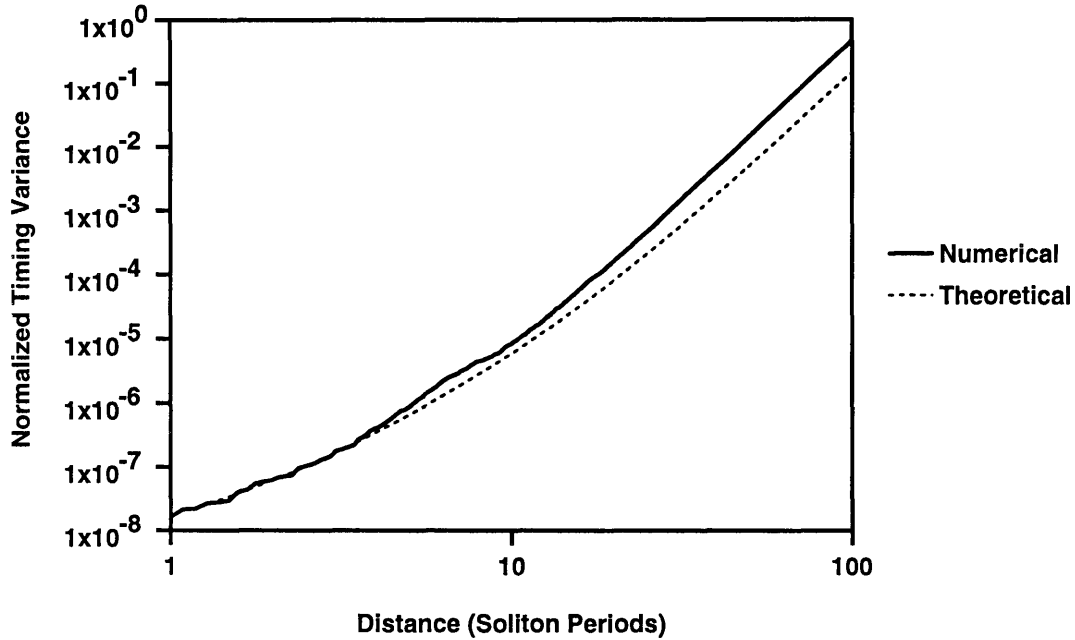


Figure 3-5: Normalized timing variance. Variance of 25 single-pulse simulations - solid curve. Dotted curve - perturbation theory. Pulse FWHM = 0.1 ps,  $D' = 0.5$  ps/nm/km. Note that the curve changes its slope from +3 to +5 at approximately  $z = 20z_0$ , which in this example is approximately 16 km.

filtering is proposed to maintain the timing of the ONEs. The stabilization of ZEROs by this method was already discussed in section 3.2.

### 3.3.3.1 Classical

When an electro-optic phase modulator is driven sinusoidally at the data rate, it changes the phase of the incoming optical field according to:

$$u_{\text{out}} = u_{\text{in}} \exp [-jM_{\text{PM}} \cos(\omega_{\text{PM}}t)] \quad (3.54)$$

The instantaneous frequency shift, which is the negative time-derivative of the phase  $\phi$ ,

$$f_i = -\frac{d\phi}{dt} \quad (3.55)$$

$$= -j\omega_{\text{PM}}M_{\text{PM}} \sin(\omega_{\text{PM}}t) \quad (3.56)$$

thus varies across the bit interval. In the presence of filtering with no detuning, the equilibrium positions for the ONEs are where the instantaneous frequency is zero (see Figure 3-6). Away from those equilibrium positions, the pulse will be alternately upshifted and downshifted in frequency, which gives rise to an oscillation in time about an equilibrium position. A filter, which damps out this oscillation, helps to guide the pulse toward the equilibrium position in an asymptotic manner.

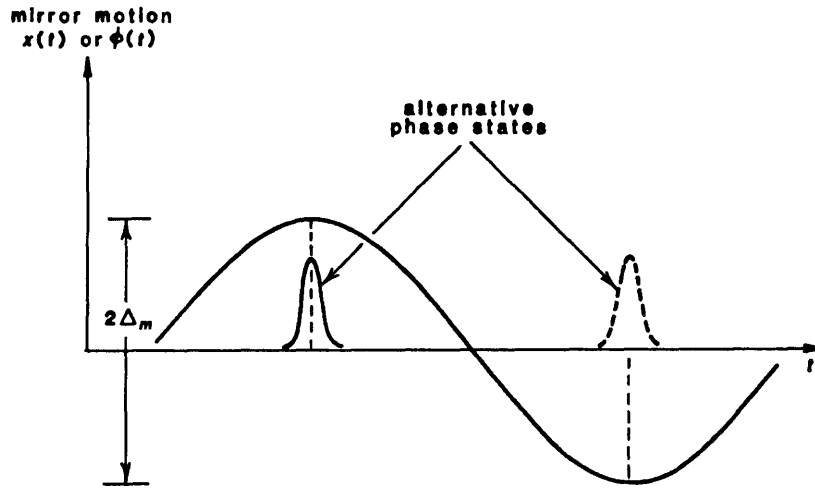


Figure 3-6: Pulse transmission through a phase modulator, after Ref. [2]. Note that  $2\Delta_m = M_{\text{PM}}$ .

Mathematically, the timing delay  $\Delta T(z)$  of a pulse satisfies the following differential equation:

$$\frac{d^2}{dz^2}\Delta T + \frac{4}{3l_f\Omega_f^2\tau^2}\frac{d}{dz}\Delta T + \frac{2DM_{\text{PM}}\omega_{\text{PM}}^2}{l_{\text{PM}}}\Delta T = \frac{32c_{\text{RD}}}{15\tau^4} + \frac{4k'''}{9l_f\Omega_f^2\tau^4} \quad (3.57)$$

One can construct an analogous system governed by Eq. (3.57), where a point mass is connected in parallel by a spring and a damper to some fixed surface (Figure 3-7). Phase modulation, which is analogous to the spring action, causes the pulse (point mass) to oscillate at some natural frequency. Meanwhile, the motion of the pulse (point mass) is damped by filtering.

Classically, when TOD and RSFS are present, the pulse will settle into a position

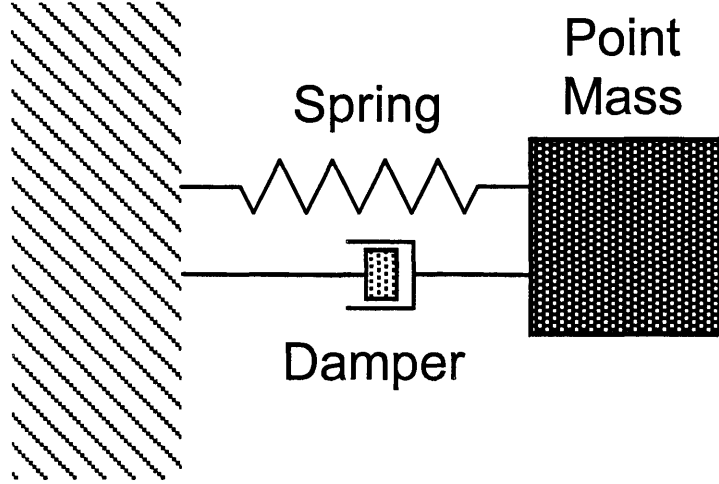


Figure 3-7: An analogous system where the position of the point mass evolves according to Eq. (3.57).

slightly offset from its natural equilibrium position. That is,

$$\lim_{z \rightarrow \infty} \Delta T(z) = \frac{l_{\text{PM}}}{2DM_{\text{PM}}\omega_{\text{PM}}^2} \left( \frac{32c_{\text{RD}}}{15\tau^4} + \frac{4k'''}{9l_f\Omega_f^2\tau^4} \right). \quad (3.58)$$

### 3.3.3.2 Stochastic

To calculate how phase modulation and filtering can reduce noise-induced timing jitter, one solves the following system of differential equations with stochastic inputs,

$$\frac{d\Delta n}{dz} = S_n(z) \quad (3.59)$$

$$\begin{aligned} \frac{d\Delta p}{dz} = & \left( \frac{16c_{\text{RD}}}{15\tau^4} \right) + \left( \frac{64c_{\text{RD}}}{15\tau^4 n_0} \right) \Delta n - \left( \frac{2}{3l_f\Omega_f^2\tau^2} \right) \Delta p \\ & - \left( \frac{M_{\text{PM}}\omega_{\text{PM}}^2}{l_{\text{PM}}} \right) \Delta T + S_p(z) \end{aligned} \quad (3.60)$$

$$\frac{d\Delta T}{dz} = \left( \frac{k'''}{6\tau^2} \right) + \left( \frac{k'''}{3\tau^2 n_0} \right) \Delta n + 2D\Delta p + S_T(z). \quad (3.61)$$

Using the Laplace transform, one can decouple the above system of differential

equations to compute the timing variance in the transformed domain,

$$\begin{aligned}
\langle \Delta T^2 \rangle &= \frac{s^2 \left( s + \frac{2}{3l_f \Omega_f^2 \tau^2} \right)^2}{\left( s^2 + \frac{2}{3l_f \Omega_f^2 \tau^2} s + \frac{M_{\text{PM}} \omega_{\text{PM}}^2}{l_{\text{PM}}} \right)^2} \left\{ \frac{2^{10} c_R^2 D^2 \delta^2 \tau^2}{225 \tau^6} \frac{\langle S_n^2 \rangle}{s^4 \left( s + \frac{2}{3l_f \Omega_f^2 \tau^2} \right)^2} \right. \\
&+ \frac{2^4 c_R k''' \delta^2 \tau^4}{45 \tau^4} \frac{\langle S_n^2 \rangle}{s^4 \left( s + \frac{2}{3l_f \Omega_f^2 \tau^2} \right)^2} + \frac{k''' \delta^2 \tau^4}{144 D^2 \tau^2} \frac{\langle S_n^2 \rangle}{s^4} \\
&+ \left. 4D^2 \frac{\langle S_p^2 \rangle}{s^2 \left( s + \frac{2}{3l_f \Omega_f^2 \tau^2} \right)^2} + \frac{\langle S_T^2 \rangle}{s^2} \right\} \quad (3.62)
\end{aligned}$$

Using the final-value theorem,

$$\lim_{z \rightarrow \infty} \langle \Delta T^2(z) \rangle = \lim_{s \rightarrow 0} s \langle \Delta T^2(s) \rangle, \quad (3.63)$$

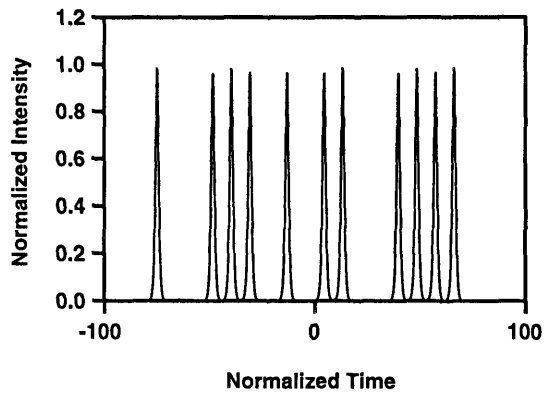
one can obtain the asymptotic behavior of  $T(z)$  for large  $z$  ( $z \gg z_0$ ). By inspection, we see that the amount of Gordon-Haus jitter is eliminated, while the Raman- and the TOD-induced timing jitter grow linearly with  $z$ :

$$\begin{aligned}
\frac{\langle \Delta T(z)^2 \rangle_{\text{RSFS, TOD}}}{\tau^2} &= \left( \frac{2^{10} c_R^2 D^2 \delta^2 \tau^2}{225 \tau^8} + \frac{2^4 c_R k''' \delta^2 \tau^4}{45 \tau^6} \frac{2}{3l_f \Omega_f^2 \tau^2} \right. \\
&+ \left. \frac{k''' \delta^2 \tau^4}{144 D^2 \tau^4} \frac{4}{9l_f^2 \Omega_f^4 \tau^4} \right) \frac{l_{\text{PM}}^2}{M_{\text{PM}}^2 \omega_{\text{PM}}^4} \langle S_n^2 \rangle z \quad (3.64)
\end{aligned}$$

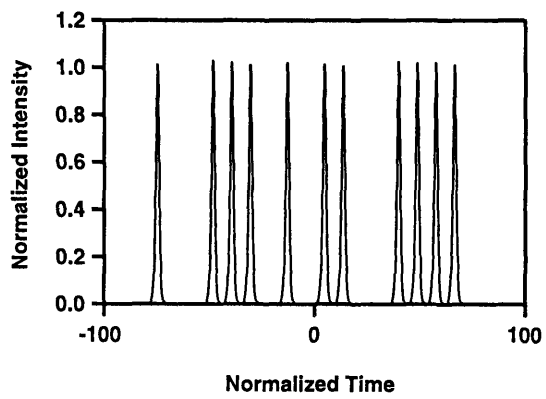
### 3.3.3.3 Numerical Simulation

We have simulated this case with a variety of parameters. An example is shown in Figure 3-8. We used a split-step Fourier algorithm with 1024 temporal gridpoints and periodic boundary conditions.

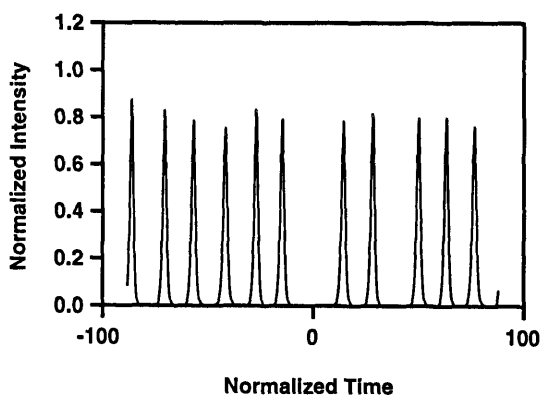
The initial condition was a 20-bit pseudorandom train of 1.8 ps soliton-like pulses (linear superposition of hyperbolic secants) at center wavelength 1.55  $\mu\text{m}$ , with a one-radian phase difference between nearest-neighbor bit intervals, and with a slight intensity modulation on the data (2 percent bit-to-bit intensity oscillation). The pulse spacing was 5:1, making for a bit rate of 111 Gb/s. The amplifier spacing



(a) initial condition



(b) after 750 km with compensation



(c) after 750 km without compensation

Figure 3-8: 111 Gb/s soliton data in storage ring with and without compensation (phase modulation and filtering). Parameters in text.

was 1 km, which is less than the 2.14 km soliton period. The fiber dispersion was 0.6 ps/nm/km anomalous, with +0.08 ps<sup>3</sup>/km TOD. The Raman time constant was taken to be 2.5 fs, and the loss was 0.2 dB/km. The phase modulator modulation depth was 0.06, and the modulation was offset in time from the initial pulses by one tenth of a bit interval, imparting an immediate small blue-shift so as to partially compensate RSFS. A scheme for achieving phase modulation at these high bit rates will be discussed elsewhere. A filter was placed opposite the amplifier in the loop. The bandwidth was 167 GHz, and the filter was offset from the pulse center frequency by +26 GHz, to partially compensate the classical RSFS shift.

The initial condition is shown in Figure 3-8(a). The data after 750 km are shown in Figure 3-8(b). The timing and intensity jitter are negligible and the classical RSFS has been overcome, through filtering and phase modulation. For comparison, we ran a simulation with no compensation but the same initial conditions. The output is shown in Figure 3-8(c). The timing information is lost without compensation.

### 3.3.4 Evolution of Systems Compensated with Intensity-dependent Absorption/Gain, Amplitude Modulation, and Filtering

#### 3.3.4.1 Case I: Filtering, AM, and FSA/G

We ran simulations for two storage rings which had the same filtering and amplitude modulation, but one had FSA ( $\gamma_3 > 0$ ) and the other had FSG ( $\gamma_3 < 0$ ). The initial condition was a 10-bit soliton-like pulse train (010011000) with 2 ps pulses at a bit rate of 50 Gbit/s.

The fast saturable gain/absorption (FSG/A) action can be realized by the principle of nonlinear polarization rotation using polarizers and waveplates [19]. The coefficient  $\gamma_3$  is calculated to be:

$$\gamma_3 = \frac{\kappa_c}{2} \sin 4\theta \sin 2\theta \cos^2 \phi \sin 2\phi \quad (3.65)$$

where  $\kappa_c = 2\delta l_{\text{Loop}}/3$ ,  $\phi$  is the order of the waveplate (e.g.  $\phi = \pi/4$  for a quarter-wave waveplate), and  $\theta$  is the angle between the transmission axis of the polarizer and the slow axis of the waveplate. To specify the amount of FSG/A, one can adjust the angle  $\theta$  of the waveplate. In this simulation, FSA was realized with  $\phi = 5\pi/16$ ,  $\theta = \pi/4$  and FSG with  $\phi = -3\pi/16$ ,  $\theta = \pi/8$ . The plots of transmission vs. intensity are shown in Figure 3-9.

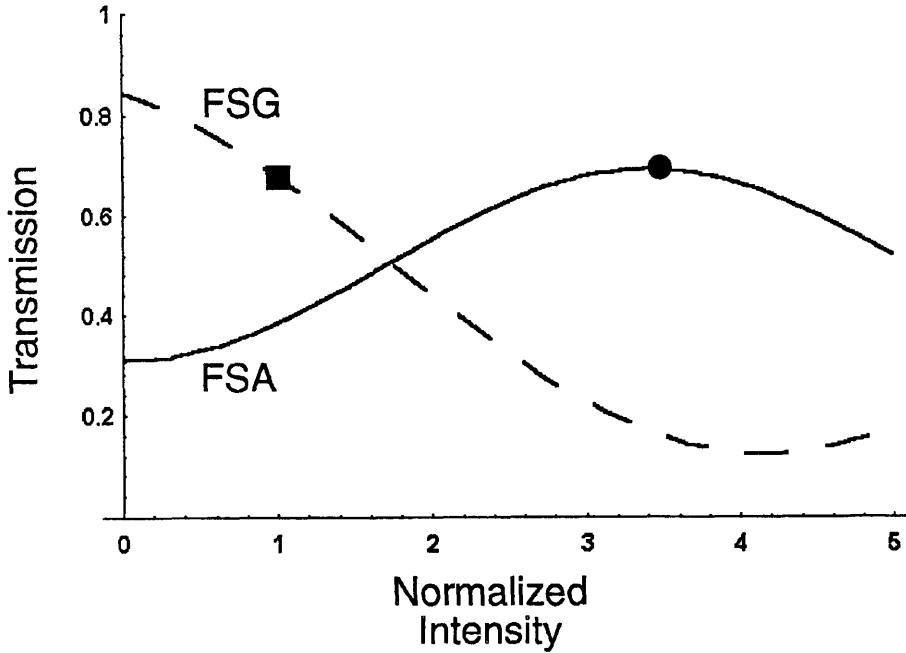


Figure 3-9: Transmission vs. intensity curves for the intensity-dependent absorption of Case I. Solid=FSA case. Dashed=FSG case. Circle indicates peak initial intensity. Square indicates peak intensity at 50 km.

Our model of a storage ring, shown in Figure 3-10, consists of an amplitude modulator, two Lorentzian filters, an amplifier with a noise figure of 2.0, a polarizer, and a quarter-wave waveplate. The total loop length is 200 m. The depth of amplitude modulation and the filter bandwidth are 0.2 and 384 GHz respectively.

For the FSG case ( $\gamma_3 < 0$ ), the initial data (shown in Figure 3-11(a)) was propagated for 50 km, and the result is shown in Figure 3-11(b). The initial ONEs broadened and became less intense. The ZEROs were observed to grow; two of them eventually becoming false ONEs. Thus, the contrast between the ZEROs and ONEs continually degraded.

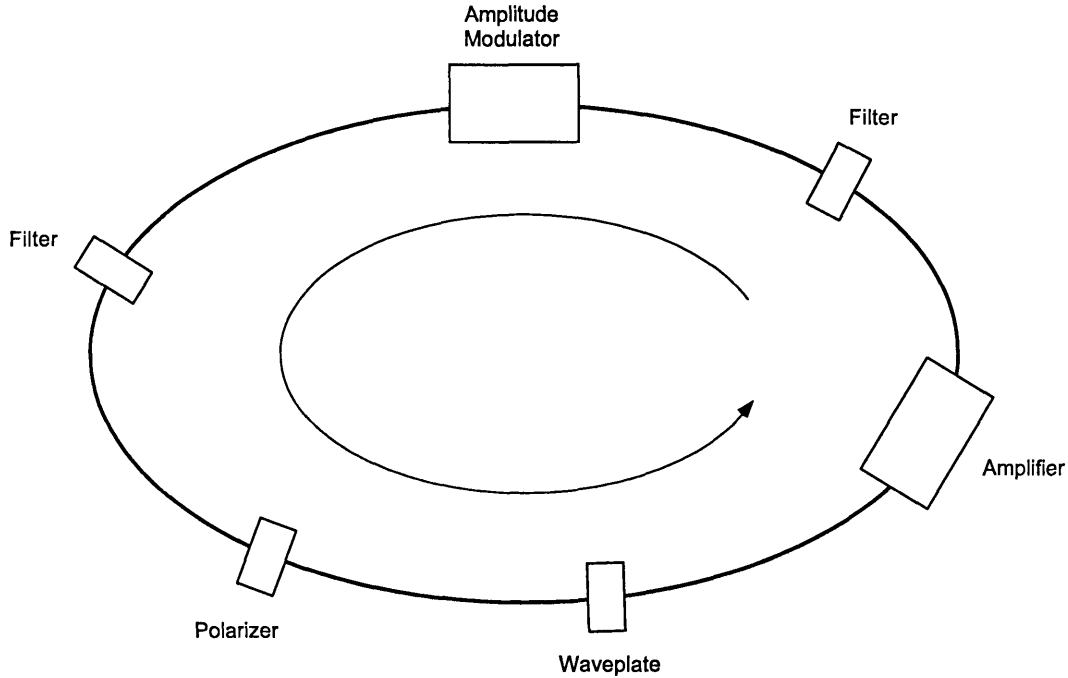


Figure 3-10: Schematic of Case I storage loop.

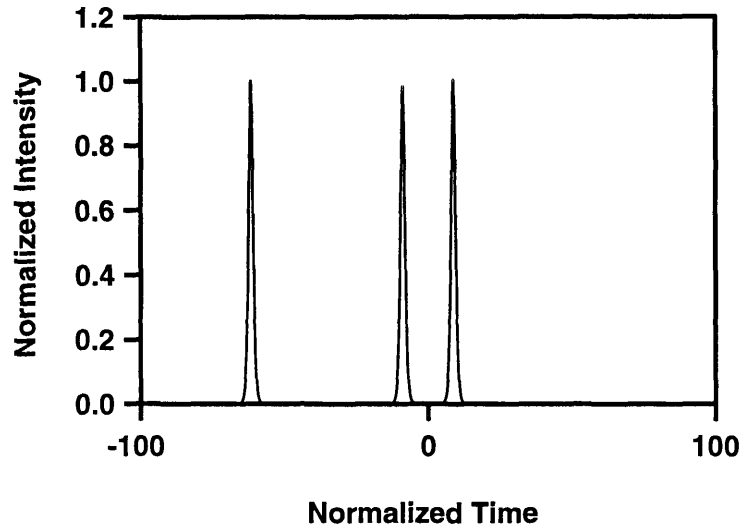
For the FSA case, the initial data of three ONEs and seven ZEROs was propagated for 2 km (10 round-trips). From Figure 3-12, one sees that the ZEROs were stable while the intensities of the ONEs fluctuated greatly, to the extent that one of the pulses was extinguished. The remaining ONEs were narrower and more delayed with respect to the amplitude modulator than the ONEs of the FSG case. The narrowness is attributed to the superior suppression of continuum which competes with the pulses (for the same gain saturation energy), and to the FSA. The time delay was due to the stronger RSFS and TOD for the shorter pulses.

### 3.3.4.2 Case II: FSA+G, AM, and Filtering

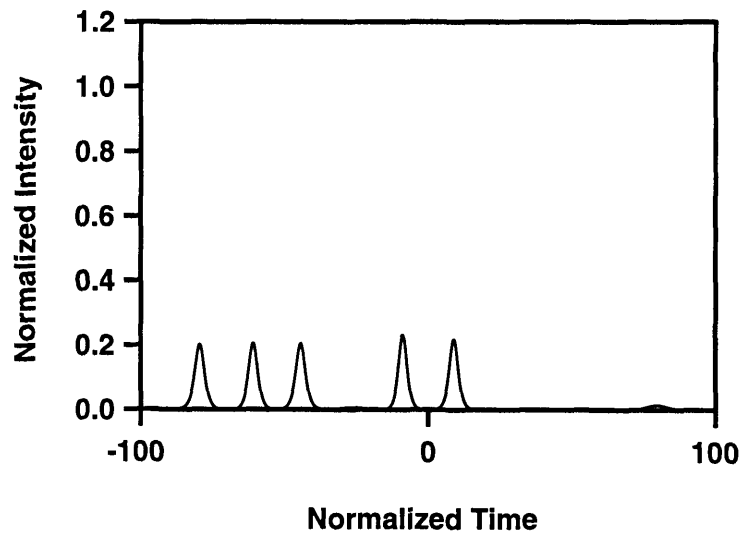
In the previous case, we found that FSA alone stabilized the ZEROs, but destabilized the ONEs. We also found that FSG alone destabilized the ZEROs and stabilized the ONEs. In this case, we consider the effect of FSA at low intensities and FSG at high intensities, which can be implemented using a  $3\lambda/16$  waveplate ( $\phi = 3\pi/16$ ) and  $\theta = \pi/8$  as shown in Figure 3-13.

A simulation was run with the above waveplate settings using a system model





(a) initial condition



(b) after 50 km

Figure 3-11: Case I with FSG. The initial ONEs broadened and became less intense. The ZEROs were observed to grow; two of them eventually becoming false ONEs.

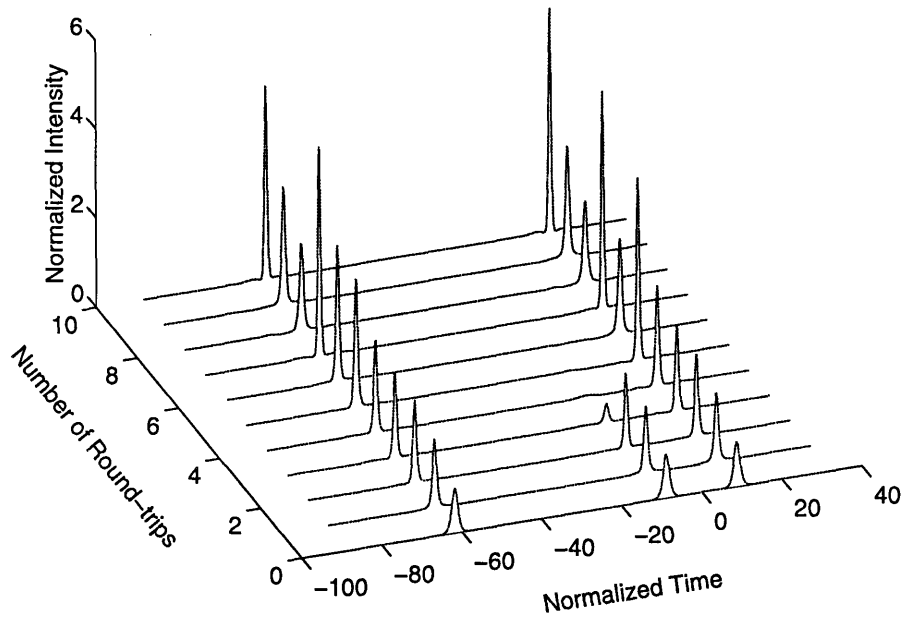


Figure 3-12: Case I with FSA. The ZEROs were stable while the intensities of the ONEs fluctuated greatly, to the extent that one of the pulses was extinguished.

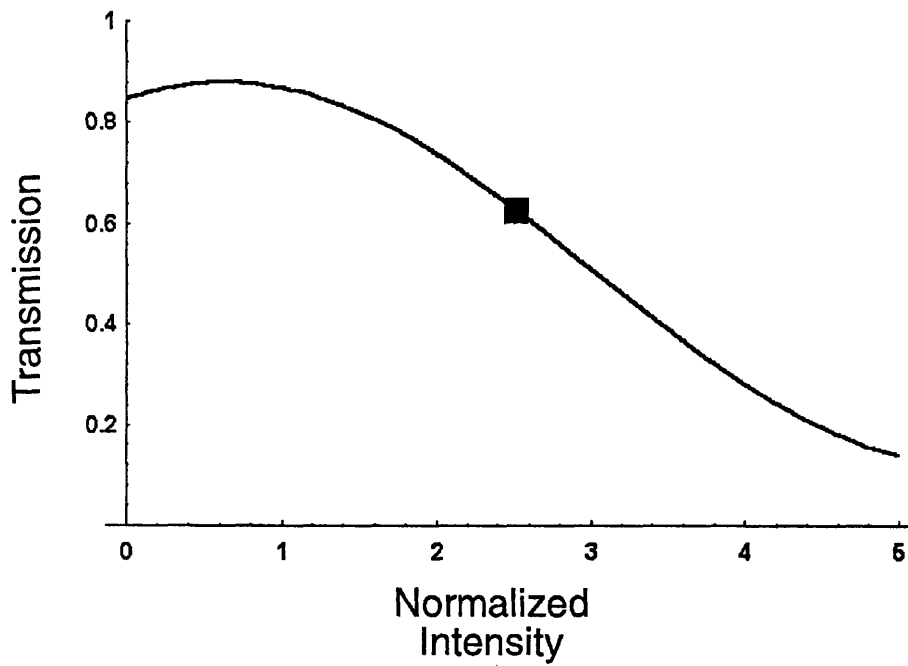


Figure 3-13: Transmission vs. intensity of the intensity-dependent absorption of Case II. Square indicates steady-state peak intensity.

otherwise identical to that used in Case I above. Steady-state operation was reached after 31 round-trips. Much smaller fluctuations of the ONEs were observed in this case than in the case of purely positive  $\gamma_3$  (Case I).

Figure 3-14 showed the data pulses after being propagated for 25 km. The contrast between the ZEROs and the ONEs was 60 dB in this FSA+G case, while it was only 20 dB (and still degrading) in the FSG case. The reason for this difference in contrast lies in the fact that FSG alone encourages low intensities; on the other hand, with suitably appropriated FSA and FSG, low intensities are discriminated while high intensities are limited and stabilized.

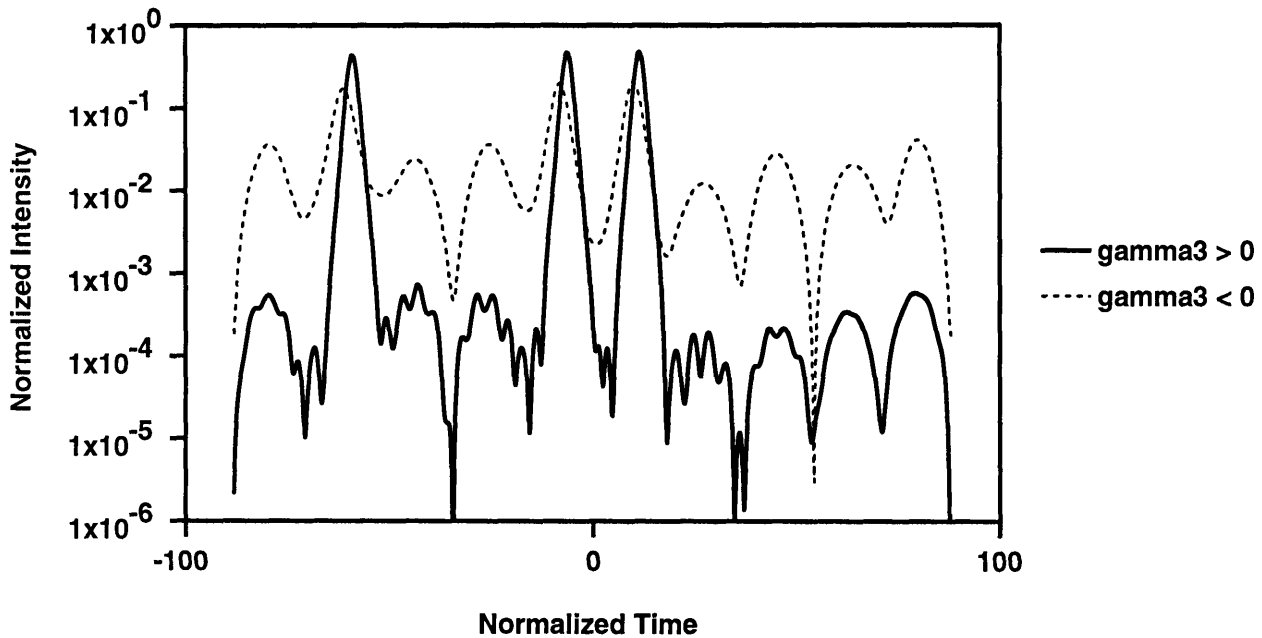


Figure 3-14: Simulation to 25 km. Solid: Case II with FSA+G. Dashed: Case I with FSG.

# Chapter 4

## Experimental Demonstration of an Optical Memory

*This work was done with Dr. Christopher R. Doerr. It is published in [41].*

### 4.1 Additive-pulse Modelocking/Limiting

Doerr et al. [3] demonstrated experimentally that an additive pulse mode-locked fiber ring laser can maintain a random pulse pattern that started from noise. The experimental setup is shown in Figure 4-1. Active modelocking is achieved by driving the Ti:LiNbO<sub>3</sub> amplitude modulator at a harmonic of the round-trip frequency. The gain medium is an erbium-doped fiber pumped by a Ti:sapphire laser at 980 nm. The nonlinear rotation of the polarization of the electric field in the fiber, followed by transmission through a polarizer, gives rise to an intracavity intensity-dependent transmission. By appropriately adjusting either the birefringent elements or the orientation of the polarization-sensitive isolator, the bias of the laser can be set for increased transmission with increasing intensity (APM,  $\gamma_3 > 0$ ), or for decreased transmission with increasing intensity (APL,  $\gamma_3 < 0$ ).

When the laser is biased such that the transmission increases with increasing

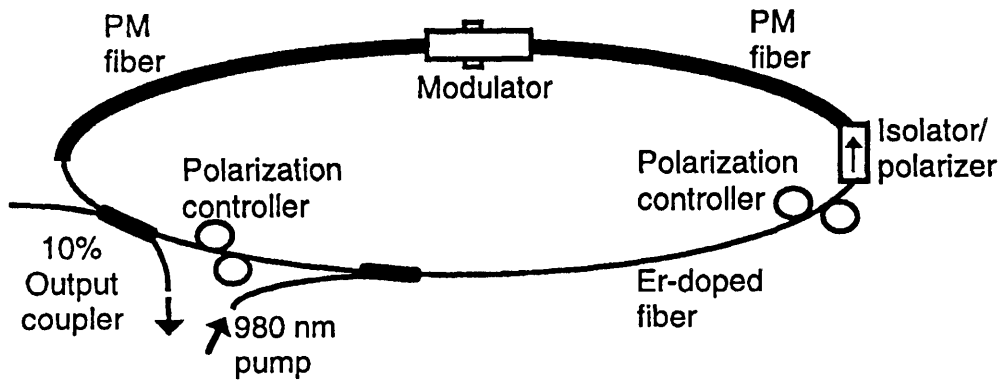


Figure 4-1: The additive-pulse limiting (APL) laser, after Ref. [3].

light intensity then decreases at a higher intensity, only few high-intensity pulses can exist in the cavity provided that the system is power-limited. Moreover, the pulses are stabilized as their peaks reach the roll-off part of the transmission curve, while low-intensity light will experience net loss. In other words, this form of bistability enhances the contrast between the ZEROs and the ONEs. Figure 4-2 shows that, out of the 17 transmission windows created by the amplitude modulator, only four are occupied. By adjusting the amount of pump power, the number of pulses (ONEs) can be varied from four to zero successively.



Figure 4-2: A random pulse pattern is maintained in the APL laser. The modulator frequency is 510 MHz (17 times the round-trip frequency). The horizontal scale is 5 ns/division, after Ref. [3].

## 4.2 Experimental Setup

Doerr's experiment revealed that his APM/L laser can maintain data patterns that are generated from noise. It is desirable to adapt his laser to store a pre-determined pulse pattern. The experimental setup is shown in Figure 4-3. It consists of two unidirectional fiber loops. The loop on the right is a pulse-pattern generator (PPG), where random data patterns are generated from intracavity noise; the loop on the left is a pulse-storage ring (PSR). Each ring contains erbium-doped fiber pumped by Ti:sapphire at 980 nm. The InGaAsP/InP semiconductor traveling-wave amplifiers (SAs) are driven at 1.0 GHz with a DC bias current. They provide gain as well creating 66 timed slots in the loop.

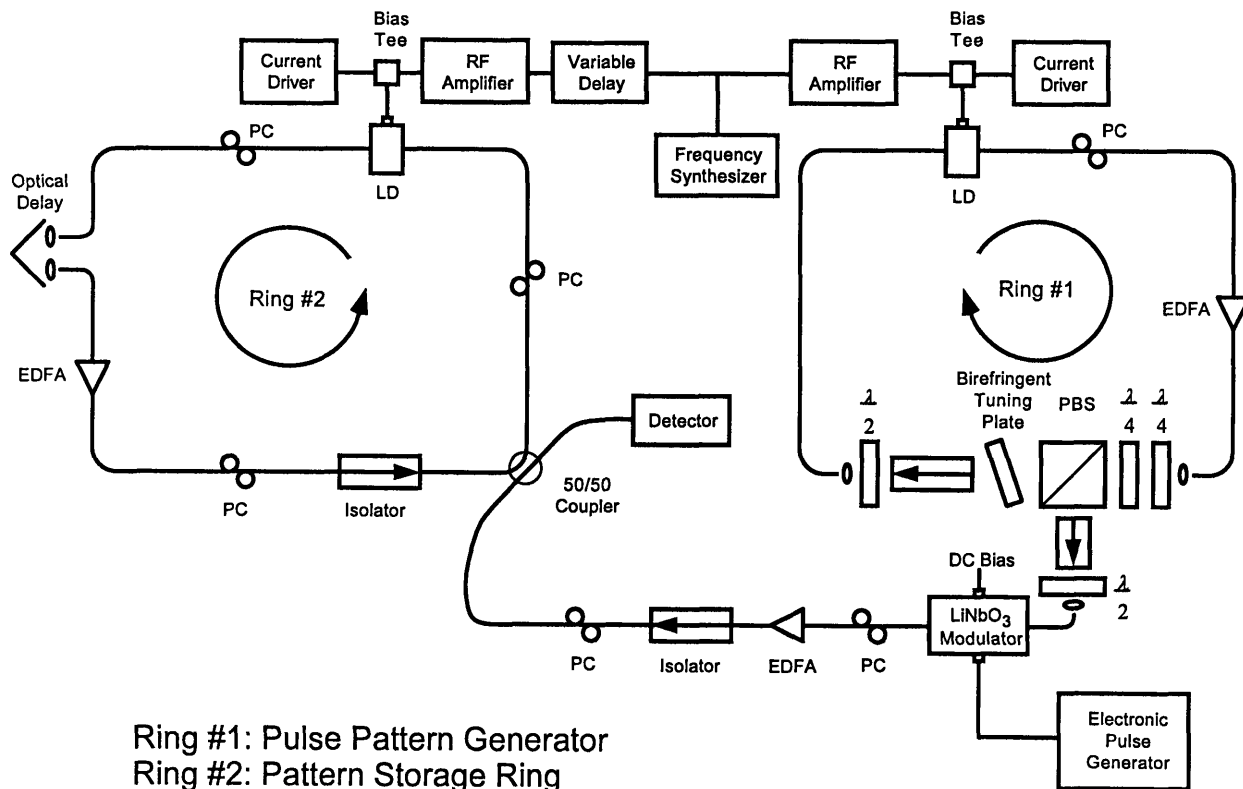


Figure 4-3: Experimental setup: EDFA, erbium-doped fiber amplifier; SA, semiconductor amplifier; PBS, polarization beam splitter;  $\lambda/2$ ,  $\lambda/4$ , half-wave and quarter-wave plates.

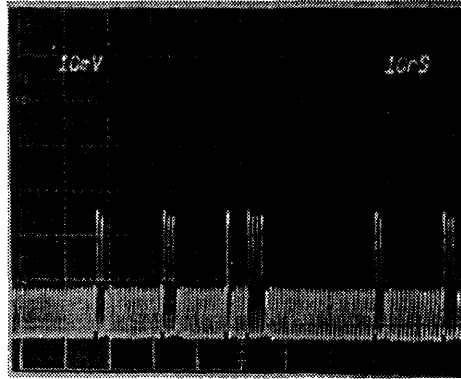
Loading of data is performed by inserting a  $\text{LiNbO}_3$  electro-optic modulator as an optical switch between the pulse-pattern generating loop and the storage loop. To

facilitate loading, one has to be able to i) synchronize the source and the storage ring while accounting for the time-of-flight of the injected pattern, iii) tune the source wavelength to match that of the storage ring, and iv) control the polarization state of the injected pulse pattern. The synchronization can be done by matching the cavity lengths of the source and the storage ring with a variable optical delay, and driving both rings with the same RF signal from a frequency synthesizer. A variable RF delay line is inserted in one arm of the RF drive to account for the propagation delay of pulses. The tuning of the pulse pattern source is achieved by rotating the birefringent plate in the ring cavity. Finally, mechanical polarization controllers can be inserted throughout the ring memory to control the injected pattern's polarization as well as setting the proper bias for nonlinear polarization rotation.

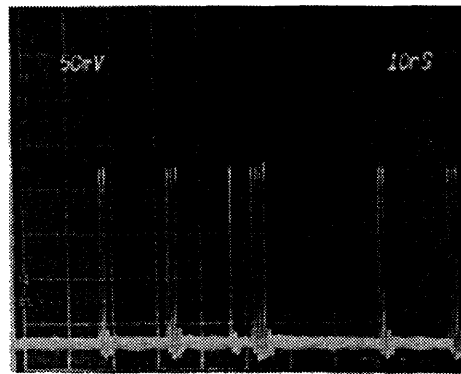
The PSR is initially empty. When a 90-ns electrical pulse is applied to the modulator, the optical switch is closed for the duration of the incoming packet of 66 bits from the PPG, allowing the packet to be loaded into the PSR. Figure 4-4 shows the oscilloscope traces of the data patterns in the PPG and in the PSR. The data packet in the PSR can be stored for as long as 30 minutes.

However, there are two problems with the current method of loading data. First, because loading is done with a passive coupler, the pulse energy of the incoming packet is, in general, smaller than the steady-state pulse energy in the storage ring. Therefore, it will take several roundtrips for the injected packet to reach equilibrium. Second, the APM bias in the storage ring is pattern-dependent. Possible solutions to these problems will be discussed in the next chapter.

The optical spectra of the PPG and the PSR, when there are four ONEs being recirculated, are shown in Figures 4-5(a) and 4-5(b) respectively. The modulations in the spectra are due to residual etalon effects in the semiconductor amplifier that cannot be eliminated completely by anti-reflection coating. Interestingly, the modulation in the optical spectrum of the PSR when it is empty (contains only low-intensity light) is almost washed out (Figure 4-5(c)), which suggests that the intracavity energy is dominated by low-coherence amplified spontaneous emission from the SA and the erbium-doped fiber amplifier.



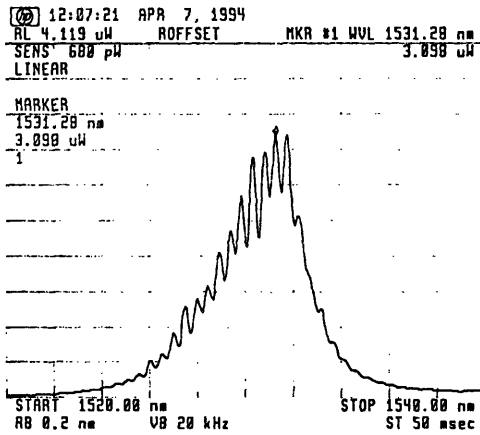
(a) oscilloscope trace of the bit pattern in the PPG (started from noise).



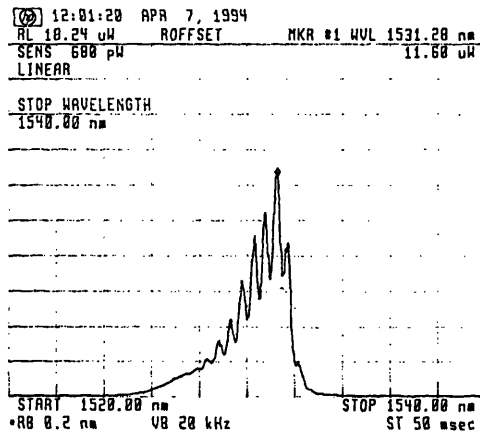
(b) oscilloscope trace of the bit pattern in the PSR after being loaded from the PPG.

Figure 4-4: Example of loading data into a storage ring by use of a 90 ns electrical gating pulse. Horizontal scale, 500 ps/division.

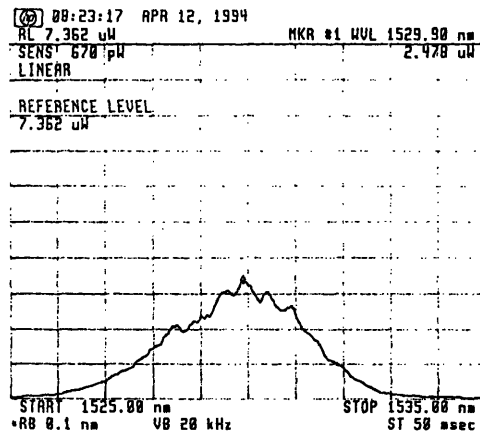




(a) optical spectrum of the PPG with four ONEs.



(b) optical spectrum of the PSR with four ONEs.



(c) optical spectrum of the empty PSR.

Figure 4-5: Optical Spectra of the PPG and the PSR.

# Chapter 5

## Conclusions and Future Work

We demonstrated stable operation of an optical pulse storage ring at 1 GHz using amplitude modulation, filtering, and APM/L action, where loading and unloading of data were done with passive couplers. In the future, an intracavity optical switch should be used so that each individual pulse can be switched into and out of the ring with a control pulse. In addition, instead of adjusting the APM bias in the storage ring to match the number of ONEs in the incoming data packet, Manchester coding should be used so that all code words have the same energy.

We propose to construct a pulse storage device in a coupled-cavity configuration that is generally known as a figure-eight laser [42,43] (Figure 5-1). It consists of a unidirectional fiber ring coupled to a nonlinear amplifying loop mirror. The amplitude modulator provides pulse timing via active modelocking, the isolator ensures the unidirectionality of propagation, and the nonlinear amplifying loop mirror (NALM) [44] provides an intensity-dependent transmission used to stabilize the ZEROs and the ONEs.

The nonlinear loop mirror operates in the following way. When a pulse enters the 50/50 coupler from the unidirectional ring, it is split into two counterpropagating pulses; one traverses the NALM in the clockwise direction and the other in the counterclockwise direction. Since the gain medium (the erbium-doped fiber) is placed asymmetrically in the loop mirror, the clockwise-propagating pulse gets amplified first, and thus acquires a larger nonlinear phase shift than the counterclockwise-

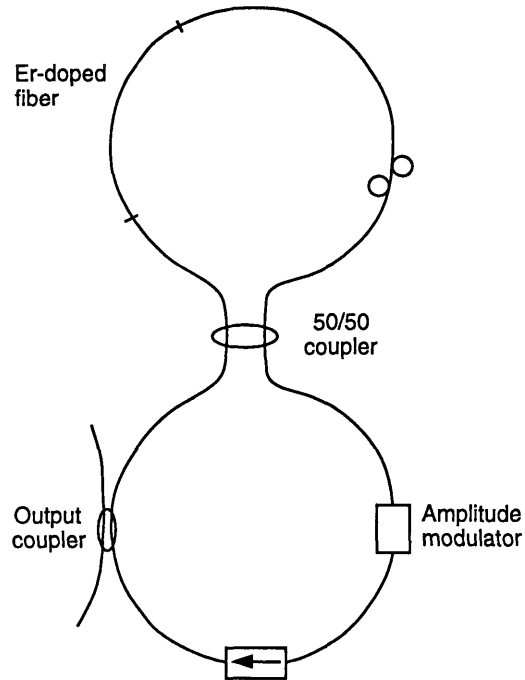


Figure 5-1: The figure-eight laser.

propagating pulse does. When the two pulses finally return to and interfere at the coupler after a roundtrip, the transmission will be a function of the incident pulse intensity. The polarization controller in the NALM is used to set the APM bias.

There are two advantages of using the figure-eight laser as a pulse storage ring. First, if one replaces the mechanical polarization controller with a variable Faraday bias, one can make the entire storage ring out of polarization maintaining fiber, thus enhancing the stability of operation. Second, all-optical switching can be performed if control pulses are coupled into the NALM. Some optical switches make use of the cross phase modulation (XPM) of the control pulse on the data pulse. Others, such as the Terahertz Optical Asymmetric Demultiplexer (TOAD) [45, 46] and the Semiconductor Laser Amplifier in a Loop Mirror (SLALOM) [47] take advantage of the fast semiconductor gain and index nonlinearities induced by the control pulse.

# Appendix A

## Normalizing the Evolution Equation

*The material in this appendix was written by Dr. John D. Moores and Farzana I. Khatri in 1988.*

### A.1 Master Equation with Group Velocity Dispersion

This is a summary of how to normalize the Master Equation. Note that it is normalized to bright solitons in media with anomalous group velocity dispersion (GVD) (and positive Kerr effect), and therefore,  $\beta_2 = -|\beta_2|$ .

The unnormalized Master Equation is as follows:

$$\begin{aligned} \frac{\partial u}{\partial z} + \sigma \frac{\partial u}{\partial t} &= \left\{ (i\psi + g - l) + \left( \frac{g}{\Omega_g^2} + \frac{1}{L_f \Omega_f^2} \right) \frac{\partial^2}{\partial t^2} \right\} u \\ &+ \left\{ i \frac{|\beta_2|}{2} \frac{\partial^2}{\partial t^2} + \frac{\beta_3}{6} \frac{\partial^3}{\partial t^3} + i \frac{\beta_4}{24} \frac{\partial^4}{\partial t^4} \right\} u - i c_R \delta_3 \frac{\partial |u|^2}{\partial t} u \\ &+ \{ (\gamma_3 + i\delta_3) |u|^2 + (\gamma_5 + i\delta_5) |u|^4 \} u. \end{aligned} \quad (\text{A.1})$$

Here  $u$  is the complex field,  $z$  is distance,  $t$  is the (possibly shifting) time coordinate,

$\sigma$  is the slip with dimensions of inverse velocity (this term can be scaled out of a single nonlinear Schrödinger equation via the shifting time coordinate, but appears in the coupled Master equations for two polarizations when the medium is birefringent - furthermore, if one of the two coupled equations is in the coordinate frame moving with its pulse, then the other equation has a slip  $\sigma = \pm\Delta n/c$ , where  $\Delta n$  is the index of refraction difference between the two polarization axes, and  $c$  is the vacuum speed of light - note that the beat length  $L_b = \Delta n/\lambda$ ),  $\psi$  is a phase shift per length,  $g$  is the (saturated) linear gain per length,  $l$  is the linear loss per length,  $\Omega_g$  is the spectral half-width at half maximum intensity of the (homogeneously-broadened) gain,  $\Omega_f$  is the spectral half-width at half maximum intensity of the net passive (static) filtering,  $L_f$  is a characteristic length for  $\Omega_f$ ,  $\beta_m, m = 2, 3, 4$  are the  $m$ th-order coefficients of group-velocity dispersion,  $c_R$  is the effective Raman relaxation time,  $\gamma_3$  is the third-order saturable absorber gain,  $\delta_3$  is the Kerr coefficient (self-phase modulation),  $\gamma_5$  is the fifth-order saturable absorber gain (usually negative, and therefore a loss), and  $\delta_5$  is the fifth-order self-phase modulation coefficient.

To normalize, first let

$$\begin{aligned} t &\longrightarrow t_n \tau \\ z &\longrightarrow z_n z_c \end{aligned}$$

where the normalized time and space variables are  $t_n$  and  $z_n$  respectively,  $\tau = 0.56729632855 \tau_{\text{FWHM}}$ ,  $\tau_{\text{FWHM}}$  is the pulse width at half-maximum intensity, and  $z_c$  is a characteristic length scale which shall be determined below, where we normalize the dispersion coefficient. The choice of time scale is such that normalized sech ( $\frac{t_n}{N}$ ) corresponds to a pulse whose FWHM is  $N\tau_{\text{FWHM}}$ , in real units.

Next, you high school sophomores should use the chain rule and figure out derivatives like this:

$$\begin{aligned} \frac{\partial u}{\partial z} &= \frac{\partial u}{\partial z_n} \frac{dz_n}{dz} = \frac{1}{z_c} \frac{\partial u}{\partial z_n} \\ \frac{\partial u}{\partial t} &= \frac{\partial u}{\partial t_n} \frac{dt_n}{dt} = \frac{1}{\tau} \frac{\partial u}{\partial t_n}. \end{aligned}$$

Similarly, with the second and third derivatives,

$$\begin{aligned}\frac{\partial^2 u}{\partial t^2} &= \frac{\partial}{\partial t} \left( \frac{1}{\tau} \frac{\partial u}{\partial t_n} \right) \frac{dt_n}{dt} = \frac{1}{\tau^2} \frac{\partial^2 u}{\partial t_n^2} \\ \frac{\partial^3 u}{\partial t^3} &= \frac{1}{\tau^3} \frac{\partial^3 u}{\partial t_n^3}.\end{aligned}$$

Making these replacements, the Master Equation becomes:

$$\begin{aligned}\frac{\partial u}{z_c \partial z_n} + \frac{\sigma}{\tau} \frac{\partial u}{\partial t_n} &= \left\{ (i\psi + g - l) + \left( \frac{g}{\Omega_g^2 \tau^2} + \frac{1}{L_f \Omega_f^2 \tau^2} \right) \frac{\partial^2}{\partial t_n^2} \right\} u \\ &+ \left\{ i \frac{|\beta_2|}{2\tau^2} \frac{\partial^2}{\partial t_n^2} + \frac{\beta_3}{6\tau^3} \frac{\partial^3}{\partial t_n^3} + i \frac{\beta_4}{24\tau^4} \frac{\partial^4}{\partial t_n^4} \right\} u \\ &- i \frac{c_R \delta_3}{\tau} \frac{\partial |u|^2}{\partial t} u \\ &+ \{ (\gamma_3 + i\delta_3) |u|^2 + (\gamma_5 + i\delta_5) |u|^4 \} u.\end{aligned}$$

Next, we divide out  $|\beta_2|/\tau^2$  so that the normalized dispersion is 1/2. This gives:

$$\begin{aligned}\frac{\tau^2}{|\beta_2| z_c} \frac{\partial u}{\partial z_n} + \frac{\sigma \tau}{|\beta_2|} \frac{\partial u}{\partial t_n} &= \left\{ (i\psi + g - l) \frac{\tau^2}{|\beta_2|} + \left( \frac{g}{\Omega_g^2 |\beta_2|} + \frac{1}{L_f \Omega_f^2 |\beta_2|} \right) \frac{\partial^2}{\partial t_n^2} \right\} u \\ &+ \left\{ i \frac{1}{2} \frac{\partial^2}{\partial t_n^2} + \frac{\beta_3}{6\tau |\beta_2|} \frac{\partial^3}{\partial t_n^3} + i \frac{\beta_4}{24\tau^2 |\beta_2|} \frac{\partial^4}{\partial t_n^4} \right\} u \\ &- i \frac{c_R \delta_3 \tau}{|\beta_2|} \frac{\partial |u|^2}{\partial t} u \\ &+ \left\{ (\gamma_3 + i\delta_3) \frac{\tau^2}{|\beta_2|} |u|^2 + (\gamma_5 + i\delta_5) \frac{\tau^2}{|\beta_2|} |u|^4 \right\} u.\end{aligned}$$

Now, if we set the coefficient for  $\partial u/\partial z_n$  to 1, we have that  $z_c = \tau^2/|\beta_2|$ . Note that

$$z_c = \frac{2z_o}{\pi}$$

where  $z_o$  is the soliton period. We would also like to normalize the Kerr coefficient to unity, for which we choose  $u = u_n/\sqrt{\delta_3 z_c}$ . Finally, we get:

$$\frac{\partial u_n}{\partial z_n} + \frac{\sigma \tau}{|\beta_2|} \frac{\partial u_n}{\partial t_n} = \left\{ (i\psi + g - l) \frac{\tau^2}{|\beta_2|} + \left( \frac{g}{\Omega_g^2 |\beta_2|} + \frac{1}{L_f \Omega_f^2 |\beta_2|} \right) \frac{\partial^2}{\partial t_n^2} \right\} u_n$$

$$\begin{aligned}
& + \left\{ i \frac{1}{2} \frac{\partial^2}{\partial t_n^2} + \frac{\beta_3}{6\tau|\beta_2|} \frac{\partial^3}{\partial t_n^3} + i \frac{\beta_4}{24\tau^2|\beta_2|} \frac{\partial^4}{\partial t_n^4} \right\} u_n \\
& - i \frac{c_R}{\tau} \frac{\partial |u_n|^2}{\partial t} u_n \\
& + \left\{ \left( \frac{\gamma_3}{\delta_3} + i \right) |u_n|^2 + (\gamma_5 + i\delta_5) \frac{|\beta_2|}{\delta_3^2 \tau^2} |u_n|^4 \right\} u_n
\end{aligned}$$

Thus, we can define normalized parameters, so that the normalized equation is of the same form as the unnormalized equation, Eq. (A.1). Thus,

$$\begin{aligned}
\sigma_n &= \frac{\sigma z_c}{\tau} \\
\psi_n &= \psi z_c \\
g_n &= g z_c \\
l_n &= l z_c \\
L_{f,n} &= \frac{L_f}{z_c} \\
\Omega_{g,n} &= \Omega_g \tau \\
\Omega_{f,n} &= \Omega_f \tau \\
\beta_{2,n} &= 1 \\
\beta_{3,n} &= \frac{\beta_3}{\tau|\beta_2|} = \frac{\beta_3 z_c}{\tau^3} \\
\beta_{4,n} &= \frac{\beta_4 z_c}{\tau^4} \\
c_{R,n} &= \frac{c_R}{\tau} \\
\gamma_{3,n} &= \frac{\gamma_3}{\delta_3} \\
\delta_{3,n} &= 1 \\
\gamma_{5,n} &= \frac{\gamma_5}{\delta_3^2 z_c} \\
\delta_{5,n} &= \frac{\delta_5}{\delta_3^2 z_c}
\end{aligned}$$

## A.2 Master Equation near Zero Group Velocity Dispersion Point

This is a summary of how to normalize the Master Equation (as in program *fiberkgn*) at a zero-group-velocity-dispersion (zero GVD) point.

The unnormalized Master Equation, with zero GVD, is as follows:

$$\begin{aligned} \frac{\partial u}{\partial z} + \sigma \frac{\partial u}{\partial t} &= \left\{ (i\psi + g - l) + \left( \frac{g}{\Omega_g^2} + \frac{1}{L_f \Omega_f^2} \right) \frac{\partial^2}{\partial t^2} \right\} u \\ &+ \left\{ \frac{\beta_3}{6} \frac{\partial^3}{\partial t^3} + i \frac{\beta_4}{24} \frac{\partial^4}{\partial t^4} \right\} u - i c_R \delta_3 \frac{\partial |u|^2}{\partial t} u \\ &+ \{ (\gamma_3 + i\delta_3) |u|^2 + (\gamma_5 + i\delta_5) |u|^4 \} u. \end{aligned}$$

Here  $u$  is the complex field,  $z$  is distance,  $t$  is the (possibly shifting) time coordinate,  $\sigma$  is the slip with dimensions of inverse velocity (this term can be scaled out of the equation via the shifting time coordinate, but appears in the coupled Master equations for two polarizations when the medium is birefringent),  $\psi$  is a phase shift per length,  $g$  is the (saturated) linear gain per length,  $l$  is the linear loss per length,  $\Omega_g$  is the spectral half-width at half maximum intensity of the (homogeneously-broadened) gain,  $\Omega_f$  is the spectral half-width at half maximum intensity of the net passive (static) filtering,  $L_f$  is a characteristic length for  $\Omega_f$ ,  $\beta_m, m = 3, 4$  are the  $m$ th-order coefficients of group-velocity dispersion,  $c_R$  is the effective Raman relaxation time,  $\gamma_3$  is the third-order saturable absorber gain,  $\delta_3$  is the Kerr coefficient (self-phase modulation),  $\gamma_5$  is the fifth-order saturable absorber gain (usually negative, and therefore a loss), and  $\delta_5$  is the fifth-order self-phase modulation coefficient.

To normalize, first let

$$\begin{aligned} t &\longrightarrow t_n \tau \\ z &\longrightarrow z_n z_3 \end{aligned}$$

where the normalized time and space variables are  $t_n$  and  $z_n$  respectively,  $\tau =$



0.56729632855  $\tau_{\text{FWHM}}$ ,  $\tau_{\text{FWHM}}$  is the pulse width at half-maximum intensity, and  $z_3$  is a characteristic length scale which shall be determined below, where we normalize the dispersion coefficient. The choice of time scale is such that normalized sech ( $\frac{t_n}{N}$ ) corresponds to a pulse whose FWHM is  $N\tau_{\text{FWHM}}$ , in real units.

Next, you high school sophomores should use the chain rule and figure out derivatives like this:

$$\begin{aligned}\frac{\partial u}{\partial z} &= \frac{\partial u}{\partial z_n} \frac{dz_n}{dz} = \frac{1}{z_3} \frac{\partial u}{\partial z_n} \\ \frac{\partial u}{\partial t} &= \frac{\partial u}{\partial t_n} \frac{dt_n}{dt} = \frac{1}{\tau} \frac{\partial u}{\partial t_n}.\end{aligned}$$

Similarly, with the second and third derivatives,

$$\begin{aligned}\frac{\partial^2 u}{\partial t^2} &= \frac{\partial}{\partial t} \left( \frac{1}{\tau} \frac{\partial u}{\partial t_n} \right) \frac{dt_n}{dt} = \frac{1}{\tau^2} \frac{\partial^2 u}{\partial t_n^2} \\ \frac{\partial^3 u}{\partial t^3} &= \frac{1}{\tau^3} \frac{\partial^3 u}{\partial t_n^3}.\end{aligned}$$

Making these replacements, the Master Equation becomes:

$$\begin{aligned}\frac{\partial u}{z_3 \partial z_n} + \frac{\sigma}{\tau} \frac{\partial u}{\partial t_n} &= \left\{ (i\psi + g - l) + \left( \frac{g}{\Omega_g^2 \tau^2} + \frac{1}{L_f \Omega_f^2 \tau^2} \right) \frac{\partial^2}{\partial t_n^2} \right\} u \\ &+ \left\{ \frac{\beta_3}{6\tau^3} \frac{\partial^3}{\partial t_n^3} + i \frac{\beta_4}{24\tau^4} \frac{\partial^4}{\partial t_n^4} \right\} u - i \frac{c_R \delta_3}{\tau} \frac{\partial |u|^2}{\partial t} u \\ &+ \{ (\gamma_3 + i\delta_3) |u|^2 + (\gamma_5 + i\delta_5) |u|^4 \} u.\end{aligned}$$

Next, we divide out  $|\beta_3|/\tau^3$  so that the normalized third-order dispersion is 1/6. This gives:

$$\begin{aligned}\frac{\tau^3}{|\beta_3| z_3} \frac{\partial u}{\partial z_n} + \frac{\sigma \tau^2}{|\beta_3|} \frac{\partial u}{\partial t_n} &= \left\{ (i\psi + g - l) \frac{\tau^3}{|\beta_3|} + \left( \frac{g\tau}{\Omega_g^2 |\beta_3|} + \frac{\tau}{L_f \Omega_f^2 |\beta_3|} \right) \frac{\partial^2}{\partial t_n^2} \right\} u \\ &+ \left\{ \frac{\beta_3}{6|\beta_3|} \frac{\partial^3}{\partial t_n^3} + i \frac{\beta_4}{24\tau |\beta_3|} \frac{\partial^4}{\partial t_n^4} \right\} u - i \frac{c_R \delta_3 \tau^2}{|\beta_3|} \frac{\partial |u|^2}{\partial t} u \\ &+ \left\{ (\gamma_3 + i\delta_3) \frac{\tau^3}{|\beta_3|} |u|^2 + (\gamma_5 + i\delta_5) \frac{\tau^3}{|\beta_3|} |u|^4 \right\} u.\end{aligned}$$

Now, if we set the coefficient for  $\partial u/\partial z_n$  to 1, we have that  $z_3 = \tau^3/|\beta_3|$ . We would also like to normalize the Kerr coefficient to unity, for which we choose  $u = u_n/\sqrt{\delta_3 z_3}$ .

Finally, we get:

$$\begin{aligned} \frac{\partial u_n}{\partial z_n} + \frac{\sigma \tau^2}{|\beta_3|} \frac{\partial u_n}{\partial t_n} &= \left\{ (i\psi + g - l) \frac{\tau^3}{|\beta_3|} + \left( \frac{g\tau}{\Omega_g^2 |\beta_3|} + \frac{\tau}{L_f \Omega_f^2 |\beta_3|} \right) \frac{\partial^2}{\partial t_n^2} \right\} u_n \\ &+ \left\{ \frac{\beta_3}{6|\beta_3|} \frac{\partial^3}{\partial t_n^3} + i \frac{\beta_4}{24\tau |\beta_3|} \frac{\partial^4}{\partial t_n^4} \right\} u_n - i \frac{c_R}{\tau} \frac{\partial |u_n|^2}{\partial t} u_n \\ &+ \left\{ \left( \frac{\gamma_3}{\delta_3} + i \right) |u_n|^2 + (\gamma_5 + i\delta_5) \frac{|\beta_3|}{\delta_3^2 \tau^3} |u_n|^4 \right\} u_n \end{aligned}$$

Thus, we can define normalized parameters, so that the normalized equation is of the same form as the unnormalized equation, Eq. (A.1). Thus,

$$\begin{aligned} \sigma_n &= \frac{\sigma z_3}{\tau} \\ \psi_n &= \psi z_3 \\ g_n &= g z_3 \\ l_n &= l z_3 \\ L_{f,n} &= \frac{L_f}{z_3} \\ \Omega_{g,n} &= \Omega_g \tau \\ \Omega_{f,n} &= \Omega_f \tau \\ \beta_{2,n} &= 0 \\ \beta_{3,n} &= 1 \\ \beta_{4,n} &= \frac{\beta_4 z_3}{\tau^4} \\ c_{R,n} &= \frac{c_R}{\tau} \\ \gamma_{3,n} &= \frac{\gamma_3}{\delta_3} \\ \delta_{3,n} &= 1 \\ \gamma_{5,n} &= \frac{\gamma_5}{\delta_3^2 z_3} \\ \delta_{5,n} &= \frac{\delta_5}{\delta_3^2 z_3} \end{aligned}$$

# Bibliography

- [1] B. J. Ainslie and C. R. Day, “A review of single-mode fibers with modified dispersion characteristics,” *J. Lightwave Tech.*, vol. 4, no. 8, pp. 967–979, August 1986.
- [2] A. E. Siegman, *Lasers*. University Science Books, 1986.
- [3] C. R. Doerr, H. A. Haus, E. P. Ippen, M. Shirasaki, and K. Tamura, “Additive pulse limiting,” *Optics Letters*, vol. 19, no. 1, pp. 31–33, January 1, 1994.
- [4] A. Hasegawa and F. Tappert, “Transmission of stationary nonlinear optical pulses in dispersive dielectric fibers. I. anomalous dispersion,” *Appl. Phys. Lett.*, vol. 23, pp. 142–144, 1973.
- [5] A. Hasegawa and Y. Kodama, “Amplification and reshaping of optical solitons in a glass fiber — I,” *Optics Letters*, vol. 7, no. 6, pp. 285–287, 1982.
- [6] Y. Kodama and A. Hasegawa, “Amplification and reshaping of optical solitons in glass fiber — II,” *Optics Letters*, vol. 7, no. 7, pp. 339–341, 1982.
- [7] A. Hasegawa, “Amplification and reshaping of optical solitons in a glass fiber — IV: use of the stimulated Raman process,” *Optics Letters*, vol. 8, no. 12, pp. 650–652, December 1983.
- [8] E. Desurvire, J. L. Zyskind, and C. R. Giles, “Design optimization for efficient erbium-doped fiber amplifiers,” *J. Lightwave Tech.*, vol. 8, no. 11, pp. 1730–1741, November 1990.

- [9] M. Nakazawa, H. Kubota, E. Yamada, and K. Suzuki, "Infinite-distance soliton transmission with soliton controls in time and frequency domains," *Electronics Letters*, vol. 28, no. 12, pp. 1099–1100, June 4, 1992.
- [10] M. Nakazawa, K. Suzuki, E. Yamada, H. Kubota, Y. Kimura, and M. Takaya, "Experimental demonstration of soliton data transmission over unlimited distances with soliton control in time and frequency domains," *Electronics Letters*, vol. 29, no. 9, pp. 729–730, April 29, 1993.
- [11] H. A. Haus and A. Mecozzi, "Long-term storage of a bit stream of solitons," *Optics Letters*, vol. 17, no. 21, pp. 1500–1502, November 1, 1992.
- [12] A. Mecozzi, J. D. Moores, H. A. Haus, and Y. Lai, "Soliton transmission control," *Optics Letters*, vol. 16, no. 23, pp. 1841–1843, December 1, 1991.
- [13] A. Mecozzi, J. D. Moores, H. A. Haus, and Y. Lai, "Modulation and filtering control of soliton transmission," *J. Opt. Soc. Am.*, vol. B9, pp. 1350–1357, August 1992.
- [14] S. B. Alexander et al., "A precompetitive consortium on wide-band all-optical networks," *J. Lightwave Tech.*, vol. 11, no. 5,6, pp. 714–735, May/June 1993.
- [15] P. E. Green, Jr., *Fiber Optic Networks*. Prentice Hall, 1993.
- [16] H. A. Haus, *Waves and Fields in Optoelectronics*. Prentice-Hall, 1984.
- [17] V. E. Zakharov and A. B. Shabat, "Exact theory of two-dimensional self focusing and one-dimensional self modulation of waves in nonlinear media," *Sov. Phys. JETP*, vol. 34, pp. 62–69, January 1972.
- [18] C. S. Gardner, J. M. Greene, M. D. Kruskal, and R. M. Miura, "Method for solving the Korteweg-de Vries equation," *Phys. Rev. Letters*, vol. 19, pp. 1095–1097, 1967.
- [19] H. A. Haus, E. P. Ippen, and K. Tamura, "Additive-pulse modelocking in fiber lasers," *IEEE J. Quantum Electronics*, vol. 30, no. 1, pp. 200–208, January 1994.

- [20] J. D. Moores, W. S. Wong, and H. A. Haus, "Stability and timing maintenance in soliton transmission and storage rings," *Optics Communications*, vol. 113, no. 1,2,3, pp. 153–175, December 15, 1994.
- [21] M. Nakazawa, H. Kubota, K. Kurokawa, and E. Yamada, "Femtosecond optical soliton propagation over long distances using adiabatic trapping and soliton standardization," *J. Opt. Soc. Am.*, vol. B8, no. 9, pp. 1811–1817, September 1991.
- [22] H. Kubota and M. Nakazawa, "Soliton transmission with long amplifier spacing under soliton control," *Electronics Letters*, vol. 29, no. 20, pp. 1780–1781, September 30, 1993.
- [23] Y. Kodama and A. Hasegawa, "Generation of asymptotically stable optical solitons and suppression of the Gordon-Haus effect," *Optics Letters*, vol. 17, no. 1, pp. 31–33, January 1, 1992.
- [24] A. Mecozzi, "Long-distance soliton transmission with filtering," *J. Opt. Soc. Am.*, vol. B10, no. 12, pp. 2321–2330, 1993.
- [25] L. F. Mollenauer, J. P. Gordon, and S. G. Evangelides, "The sliding-frequency guiding filter: an improved form of soliton jitter control," *Optics Letters*, vol. 17, no. 22, pp. 1575–1577, November 15, 1992.
- [26] M. Romagnoli, S. Wabnitz, and M. Midrio, "Bandwidth limits of soliton transmission with sliding filters," *Optics Communications*, vol. 104, no. 4,5,6, pp. 293–297, January 1, 1994.
- [27] Y. Kodama and S. Wabnitz, "Analysis of soliton stability and interactions with sliding filters," *Optics Letters*, vol. 19, no. 3, pp. 162–164, February 1, 1994.
- [28] S. Wabnitz, "Suppression of soliton interactions by phase modulation," *Electronics Letters*, vol. 29, no. 19, pp. 1711–1713, September 16, 1993.
- [29] S. Wabnitz, "Suppression of interactions in a phase-locked soliton optical memory," *Optics Letters*, vol. 18, no. 8, pp. 601–603, April 15, 1993.

- [30] N. J. Smith, K. J. Blow, W. J. Firth, and K. Smith, "Soliton dynamics in the presence of phase modulators," *Optics Communications*, vol. 102, no. 3,4, pp. 324–328, October 1, 1993.
- [31] H. A. Haus, J. G. Fujimoto, and E. P. Ippen, "Structures for additive pulse mode locking," *J. Opt. Soc. Am.*, vol. B8, no. 10, pp. 2068–2076, October 1991.
- [32] S. G. Evangelides, L. F. Mollenauer, J. P. Gordon, and N. S. Bergano, "Polarization multiplexing with solitons," *J. Lightwave Tech.*, vol. 10, no. 1, pp. 28–35, January 1992.
- [33] H. A. Haus, "Quantum noise in a solitonlike repeater system," *J. Opt. Soc. Am.*, vol. B8, no. 5, pp. 1122–1126, May 1991.
- [34] L. F. Mollenauer, S. G. Evangelides, and H. A. Haus, "Long-distance soliton propagation using lumped amplifiers and dispersion shifted fiber," *J. Lightwave Tech.*, vol. 9, no. 2, pp. 194–197, February 1991.
- [35] J. D. Moores, "On the Ginzburg-Landau laser mode-locking model with fifth-order saturable absorber term," *Optics Communications*, vol. 96, no. 1,2,3, pp. 65–70, February 1, 1993.
- [36] M. Matsumoto and A. Hasegawa, "Numerical study of the reduction of instability in bandwidth-limited amplified soliton transmission," *Optics Letters*, vol. 18, no. 11, pp. 897–899, June 1, 1993.
- [37] J. P. Gordon and L. F. Mollenauer, "Effects of fiber nonlinearities and amplifier spacing on ultra-long distance transmission," *J. Lightwave Tech.*, vol. 9, no. 2, pp. 170–173, February 1991.
- [38] H. A. Haus and Y. Lai, "Quantum theory of soliton squeezing: a linearized approach," *J. Opt. Soc. Am.*, vol. B7, no. 3, pp. 386–392, March 1990.
- [39] D. J. Kaup, "Perturbation theory for solitons in optical fibers," *Phys. Rev. A*, vol. 42, no. 9, pp. 5689–5694, 1990.

- [40] K. J. Blow, N. J. Doran, and D. Wood, "Suppression of the soliton self-frequency shift by bandwidth-limited amplification," *J. Opt. Soc. Am.*, vol. B5, no. 6, pp. 1301–1304, June 1988.
- [41] C. R. Doerr, W. S. Wong, H. A. Haus, and E. P. Ippen, "Additive-pulse modelocking/limiting storage ring," *Optics Letters*, vol. 19, no. 21, pp. 1747–1749, November 1, 1994.
- [42] D. J. Richardson, R. I. Laming, D. N. Payne, V. Matsas, and M. W. Phillips, "Selfstarting passively modelocked erbium fibre ring laser based on the amplifying sagnac switch," *Electronics Letters*, vol. 27, no. 6, pp. 542–544, March 14, 1991.
- [43] I. N. Duling, III, "Subpicosecond all-fibre erbium laser," *Electronics Letters*, vol. 27, no. 6, pp. 544–545, March 14, 1991.
- [44] M. E. Fermann, F. Haberl, M. Hofer, and H. Hochreiter, "Nonlinear amplifying loop mirror," *Optics Letters*, vol. 15, no. 13, pp. 752–754, July 1, 1990.
- [45] J. P. Sokoloff, P. R. Prucnal, I. Glesk, and M. Kane, "A Terahertz optical asymmetric demultiplexer (TOAD)," *IEEE Photonics Tech. Letters*, vol. 5, no. 7, pp. 787–790, July 1993.
- [46] J. P. Sokoloff, I. Glesk, P. R. Prucnal, and R. K. Boncek, "Performance of a 50 Gbit/s optical time domain multiplexed system using a terahertz optical asymmetric demultiplexer," *IEEE Photonics Tech. Letters*, vol. 6, no. 2, pp. 98–100, January 1994.
- [47] M. Eiselt, "Optical loop mirror with semiconductor laser amplifier," *Electronics Letters*, vol. 28, pp. 1505–1507, July 30, 1992.